UNIVERSITY OF TURKU

SYNTHETIC HACKMANITES AND THEIR OPTICAL PROPERTIES – FROM THEORY TO APPLICATIONS

Isabella Norrbo

UNIVERSITY OF TURKU

SYNTHETIC HACKMANITES AND THEIR OPTICAL PROPERTIES – FROM THEORY TO APPLICATIONS

Isabella Norrbo

University of Turku

Faculty of Science and Engineering
Department of Chemistry
Laboratory of Materials Chemistry and Chemical Analysis
University of Turku Graduate School
Doctoral Programme in Physical and Chemical Sciences

Supervised by

Adjunct Professor Mika Lastusaari
Department of Chemistry
Laboratory of Materials Chemistry and Chemical Analysis
University of Turku
FI-20014 Turku, Finland

Reviewed by

Associate Professor Henrik Friis
Department of research and
collections
University of Oslo, Natural History
Museum
NO-0318 Oslo, Norway

Professor John S. O. Evans
Department of Chemistry,
Durham University
DH1 3LE, Durham, UK

Opponent

Professor Mark T. Weller
Cardiff University
CF10 3AT, Wales, UK

"The only place success comes before work is in the dictionary."
-Stubby Currence

Abstract

UNIVERSITY OF TURKU

Faculty of Science and Engineering, Department of Chemistry, Laboratory of Materials Chemistry and Chemical Analysis

NORRBO, ISABELLA: Synthetic hackmanites and their optical properties – from theory to applications
Doctoral thesis, 147 p.
March, 2019

Synthetic hackmanite is a material that resembles the natural mineral, hackmanite. The structure of hackmanite, $Na_8Al_6Si_6O_{24}(Cl,S)_2$, together with its simple preparation with solid state synthesis enables the doping of different ions into the hackmanite matrix, resulting in materials with a wide variety of optical properties.

The synthetic hackmanites show photoluminescence, persistent luminescence and photochromism, when excited with different wavelengths. During this thesis work, a synthetic hackmanite material showing up-conversion luminescence was also prepared.

This thesis focuses on the optical properties of synthetic hackmanites and their mechanisms. A detailed mechanism for persistent luminescence as well as photochromism in synthetic hackmanite materials is presented. Also, a new method called thermotenebrescence is introduced. This method can be used to study the energetics of photochromism.

With wide and tunable optical properties, cheap production and the fact that synthetic hackmanites do not include any heavy metals or toxic elements, many possible applications can be presented for the materials and they are listed in the end of the thesis.

Tiivistelmä

TURUN YLIOPISTO

Luonnontieteiden ja tekniikan tiedekunta, Kemian laitos, Materiaalikemian ja kemiallisen analyysin laboratorio

NORRBO, ISABELLA: Synteettiset hackmaniitit ja niiden optiset ominaisuudet – teoriasta käyttökohteisiin
Väitöskirja, 147 s.
Maaliskuu, 2019

Synteettinen hackmaniitti on mineraali, joka muistuttaa luonnon mineraalia, hackmaniittia. Hackmaniitin rakenteen ($Na_8Al_6Si_6O_{24}(Cl,S)_2$) ja helpon valmistusmenetelmän ansioista synteettisten hackmaniittien rakenteeseen voidaan seostaa erilaisia ioneja, jolloin materiaalille saadaan laaja kirjo erilaisia optisia ominaisuuksia.

Kun synteettisiä hackmaniitteja viritetään eri aallonpituuksilla, voidaan havaita luminesenssia, viivästynyttä luminesenssia ja fotokromismia. Tämän väitöskirjatyön aikana valmistettiin myös synteettinen hackmaniitti, jossa havaitaan käänteisviritteistä luminesenssia.

Tämä väitöskirja keskittyy synteettisten hackmaniittien optisiin ominaisuuksiin ja mekanismeihin ominaisuuksien takana. Yksityiskohtainen mekanismi esitetään sekä viivästyneelle luminesenssille että fotokromismille synteettisessä hackmaniittimateriaalissa. Lisäksi esitellään uusi menetelmä, jota kutsutaan termotenebresenssiksi. Tätä menetelmää voidaan käyttää tutkittaessa fotokromismin energetiikkaa.

Koska synteettisillä hackmaniiteilla on monia, muokattavia optisia ominaisuuksia, niiden valmistus on halpaa eivätkä ne sisällä raskasmetalleja tai myrkyllisiä alkuaineita, voidaan niille esittää monia mahdollisia käyttökohteita. Tällaisia käyttökohteita on listattuna väitöskirjan lopussa.

Table of Contents

Preface

Here I am with a ready doctoral thesis that has my name on the cover. I was not supposed to ever get this far and now, here I am. I could not have done it all by myself so I'll now take a moment to remember and thank the people who have helped me along the way and pushed me to the right direction.

First I want to thank my supervisor, adjunct Professor Mika Lastusaari for the support and guidance along the way. It has been a pleasure to work with you and most of the interesting findings during the research resulted from your ideas. You offered me the chance to do PhD studies, you have sat with me in countless meetings and you have given me help and valuable information and patiently repeated it when I forgot most of it in 5 minutes. I also want to thank Professor John Evans and associate Professor Henrik Friis for the pre-examination of my thesis and the insight and helpful comments on the thesis. I then want to thank Professor Mark T. Weller for agreeing to be my opponent.

Next I want to thank all the co-author for their valuable contributions to our joint publications. Especially I want to thank Doctor Jari Sinkkonen for the help in measuring and interpreting NMR results, Doctor Iko Hyppänen for the help with measurement setups for up-conversion and photochromism measurements and Doctor Pawel Gluchowski for guiding me in the very beginning of my research career. Great thanks goes also to all the other co-authors, Petriina Paturi, Tero Laihinen, Pekka Laukkanen, Jaakko Mäkelä, Fikret Mamedov, Hellen Santos, Minnea Tuomisto, Antti Viinikanoja, José Carvalho, Markus Peurla,

Hanna Helminen, Sari Pihlasalo, Harri Härmä, Antton Curutchet, Ari Kuusisto, Erik Wetterskog and Tangui Le Bahers.

I want to give my gratitude to Professor Carita Kvarnström for being in charge for all the official things regarding my doctoral studies. You had time for me in your busy schedule, when something was needed. I also want to thank Kari Loikas and Mauri Nauma for the help during the work. I did not find a thing that was so broken you could not either fix it or build something similar so that I could continue my research. Thank you for being here supporting us throughout the years.

The work could not have been done with such joy if it was not for the great research group we have. Because of that, I want to thank the current and former members of the Inorganic Materials Chemistry research group, Doctor Ari Lehtonen, Doctor Tero Laihinen, Doctor Hellen Santos, Doctor Anssi Peuronen, Esko Salojärvi, Pasi Salonen, Cecilia Agamah, Sobia Rashid and all the Bachelors and Masters students we have had during the years. From the research group I want to give special thanks to my wonderful officemates Emilia Palo and Minnea Tuomisto. You were always there for me when I needed something and together we figured out the problems this journey put in front of us. We made some fun memories at work and the funniest ones, of course, outside of work. Minnea gets special thanks for the company during lunch breaks and Emilia must be thanked for the late night conversations and for organizing all the after works and pre-Christmas parties to lift the spirit of the whole research group.

Our research group has had the privilege of hosting Brazilian visitors that have left their mark in our research and our lives. Doctor Jose Carvalho and Doctor Liana Namakura, the year you spent here was an inspiring one. I was pleased to be able to work with you and spend my free time with you showing you the parties and other fun stuff you can do in Finland. We also had the joy of having Doctor Hellen Santos here for her doctoral studies. You soon become more of a friend than a workmate for me. Your positive attitude and your unique laughter have brightened up my life countless times.

When looking back at things that let me here, I also want to thank my High School chemistry teacher, Tuomas Yli-Kokko. You awoke the curiosity in chemistry inside of me. Your lectures and laboratory works combined with the personal stories you told us from your chemistry studies are a big reason I ended up here in the first place, so thank you for that.

The work needs to be balanced with a proper amount of free time. In this, I have been lucky to find so great friends to spend this time with. First I want to thank Salla Lahdenpohja. Not only did you read the first draft of this work and point out to me all the silly mistakes I made, you have been supporting me all the way up to this point. We were lucky to be in the same group the day we started university. From there we went to all the parties there were and if there were none, we arranged our own. We have been on this journey together from the Bachelors' degree all the way to here and hopefully for years to come - thank you. University has also blessed me with other great friends, Tuuli Kettunen, Ville Eskonen, Milla Suominen, Eerik Salonen, Aleksi Nyqvist, Eerik Piirtola and many more. Thank you for the times shared and memories made together.

I also want to thank my friends from before university times. Even though we don't see that often anymore you are still an important part of my life. Iida-Sofia Yli-Kokko, Anna-Riikka Perkiö, Terhi Koskiniemi, Aino Ketola and Anna Herrala, we share the fun memories from the trips we took and I always enjoy the times we get together. Terhi Myllymäki, you have been my friend the longest and you have seen me grow, hopefully for the better. After all this time our friendship still stays and for that I am thankful.

Now, I also want to thank my family for giving me courage and always supporting me in whatever I wanted to do. My mother Ulla and my father Peter, you have been there for me always when I needed it and you have been making sure I have everything I need during these years, even if I didn't know I needed it myself. My sister Marlena, my grandfather Otto and late grandmother Vappu, you always made me smile when I came home to visit. My sister Mikaela, I hope you know how important you are to me. You are a sister and a friend and it is

great to have a family member like you living close. I also want to thank all my other relatives for the support I got during the years.

Last, I want to thank Vesa for being there for me all the time. You listened to my problems and waited patiently when my work and hobbies took almost all of my time, making sure I was happy. I love you more than I remember to tell you and I am so lucky to have you in my life.

Turku, April 9, 2019   Isabella Norrbo

List of original publications

The experimental part of the thesis is based on the following publications and supplementary unpublished results. The publications can be found at the end and are referred to in the text by their Roman numerals.

I.   Norrbo, I., Gluchowski, P., Paturi, P., Sinkkonen, J., and Lastusaari, M., Persistent Luminescence of Tenebrescent $Na_8Al_6Si_6O_{24}(Cl,S)_2$: Multifunctional Optical Markers, *Inorg. Chem.*, **54**, (2015), 7717–7724.

II.   Norrbo, I., Gluchowski, P., Hyppänen, I., Laihinen, T., Laukkanen, P., Mäkelä, J., Mamedov, F., Santos, H.S., Sinkkonen, J., Tuomisto, M., Viinikanoja, A., and Lastusaari, M., Mechanisms of tenebrescence and persistent luminescence in synthetic hackmanite $Na_8Al_6Si_6O_{24}(Cl,S)_2$, *ACS Appl. Mater. Interfaces*, **8**, (2016), 11592–11602.

III.   Norrbo, I., Carvalho, J., Laukkanen, P., Mäkelä, J., Mamedov, F., Peurla, M., Helminen, H., Pihlasalo, S., Härmä, H., Sinkkonen, J., and Lastusaari, M., Lanthanide and Heavy Metal Free Long White Persistent Luminescence from Ti Doped Li-Hackmanite: A Versatile, Low-Cost Material, *Adv. Funct. Mater.*, **27**, (2017), 1606547.

IV.   Norrbo, I., Curutchet, A., Kuusisto, A., Mäkelä, J., Laukkanen, P., Paturi, P., Laihinien, T., Sinkkonen, J., Wetterskog, E., Mamedov, F., Le Bahers, T., and Lastusaari, M., Solar UV index and UV dose determination with photochromic hackmanites: From the assessment of the fundamental properties to the device, *Mater. Horiz.,* **5**, (2018), 569–576.

V.   Norrbo, I., Hyppänen, I., and Lastusaari, M., Up-conversion luminescence – a new property in tenebrescenct and persistent luminescent hackmanites, *J. Lumin.*, **191**, (2017), 28–34.

Abbreviations and symbols

□	vacancy in the chemical structure
3D	three dimensional
a.u.	arbitrary unit
DFT	density functional theory
Dist.	distribution
DOS	density of states
E	energy
E_T	trap energy
EPR	electron paramagnetic resonance
F level	energy level in photochromic material arising from defects
FTIR	Fourier-transform infrared
g	gravitational force
ICP-MS	inductively coupled plasma-mass spectrometry
IR	infrared
k	Boltzmann constant
LED	light emitting diode
MAS	magic angle spinning
MW	microwave
NMR	nuclear magnetic resonance
PBC	periodic boundary condition
PeL	persistent luminescence
PL	photoluminescence
PMT	photomultiplier tube
RGB	red, green and blue
SCF	self-consistent field
SEM-EDS	scanning electron microscopy - energy-dispersive X-ray spectroscopy
T	temperature

TEM	transmission electron microscopy
TL	thermoluminescence
TT	thermotenebrescence
U level	energy level in photochromic material arising from dopants or impurities
UV	ultraviolet
V_{Cl}	chloride vacancy
V_O	oxygen vacancy
VOM	volt-ohm-milliammeter
XPD	X-ray powder diffraction
XPS	X-ray photoelectron spectroscopy
XRF	X-ray fluorescence

1. Introduction

Synthetic hackmanites are materials that are prepared synthetically to mimic the natural mineral, hackmanite. The mineral hackmanite $Na_8Al_6Si_6O_{24}(Cl,S)_2$ belongs to the sodalite $(Na_8Al_6Si_6O_{24}Cl_2)$ family together with nosean $Na_8Al_6Si_6O_{24}(SO_4)$, haüyne $(Na,Ca)_{4-8}Al_6Si_6O_{24}(SO_4,S)_{1-2}$, lazurite $(Na,Ca)_8Al_6Si_6O_{24}(SO_4,S,Cl_2)$, tugtupite $Na_8Be_2Al_2Si_8O_{24}(Cl,S)_2$, danalite $Fe_8Be_6(Si_6O_{24})S_2$, helvite $Mn_8Be_6(Si_6O_{24})S_2$ and genthelvite $Zn_8Be_6(Si_6O_{24})S_2$ [1]. Hackmanite is defined as the photochromic, sulfur containing variety of sodalite [2–4]. Thus, photochromism *i.e.* the ability to change color when absorbing radiation of a suitable wavelength is characteristic to hackmanites.

Despite the first official record of natural hackmanites being from 1834 [5], it was not until 1920s that the research of synthetic hackmanites started, led by Frans Jaeger [6] who studied synthetic hackmanites for their photochromic properties and was also able to solve their crystal structure. After Jager, there were only a couple of publications in 1950s, 1960s and 1970s (*e.g.* [7–9]) but none of the research groups published more than one publication. Weller published a few publications in the beginning of 2000s [10,11] but after that, there were again just single articles published (*e.g.* [12]).

In photochromism, the material absorbs energy forming a color center. The energy absorption of the color center gives the material a different color from its original one. When the color center absorbs a photon with high enough energy, the color center discharges and the material loses its color. If not enough energy

is present to discharge the color center, the obtained color will last. This coloration and discoloration cycle can be repeated indefinitely.

In addition to photochromism, synthetic hackmanites sometimes also exhibit photoluminescence (PL). During the course of this thesis work, strong persistent luminescence (PeL) was also obtained from synthetic hackmanites. PeL is in a way a similar property to photochromism, because also here energy is first absorbed, stored and then released. In PL, the energy absorption and the release happen successively, without the energy being stored in between [I,III].

This work focused on preparing synthetic hackmanite materials using solid state synthesis, since it is the most repeatable way to produce synthetic hackmanite materials with favorable optical properties despite the long synthesis time. The prepared materials were then studied for their optical properties and the mechanisms behind the properties [I-IV].

X-ray powder diffraction (XPD), X-ray fluorescence (XRF) and nuclear magnetic resonance (NMR) measurements were used, among other methods to characterize the prepared materials. After this, the luminescent and photochromic properties of the synthesized materials were studied using, for example, thermoluminescence (TL), luminance and reflectance measurements.

During the course of the work, a mechanism was presented for both PeL and photochromism in synthetic hackmanite materials [II]. With the knowledge of the mechanism, new synthetic hackmanite materials were prepared with improved optical properties. As a result, a synthetic hackmanite material with a record long white PeL was synthesized and characterized [III].

With the new knowledge and new, versatile hackmanite materials several possible applications for synthetic hackmanite materials were proposed, including personal ultraviolet (UV) dose monitoring, [IV] use as a non-specific label in luminescence diagnostics [III] and a hackmanite based optical sensor with multiple possible signals from one material [V].

2. Literature review

2.1. Hackmanite mineral

Hackmanite is a mineral that can be found in nature, *e.g.* in Afghanistan [13], Brazil [14], Canada [15] and Greenland [3]. By definition, hackmanite is the photochromic variety of sodalite, with the composition of $Na_8Al_6Si_6O_{24}Cl_2$ [7]. In other references, the definition of hackmanite also includes the presence of sulfur (*i.e.* $Na_8Al_6Si_6O_{24}(Cl,S)_2$) [3,10,11]. It has been named after a Finnish geologist, Victor Hackman [12].

Hackmanite has a cubic crystal structure with the space group $P\bar{4}3n$ [16]. The unit cell axis length of hackmanite is usually referred to be 8.877 Å, as calculated for a natural hackmanite from Quebec [10,15]. Hackmanite structure consists of SiO_4 and AlO_4 tetrahedra that are linked together to form a three dimensional (3D) network structure [11]. The tetrahedra form four-membered rings of alternating SiO_4 and AlO_4 units. The four-membered rings are then linked together forming six-membered rings and thus, the 3D cubo-octahedral structure of hackmanite is formed (**Figure 1**) [17]. The 3D framework hosts the Na and Cl atoms inside. The Na atom is coordinated to three framework oxygens and one Cl atom. The Cl atom on the other hand is coordinated tetrahedrally to four Na atoms. When sulfur is present, it replaces one Cl and creates a chloride vacancy (V_{Cl}) to balance the different charges with the anions. [18]
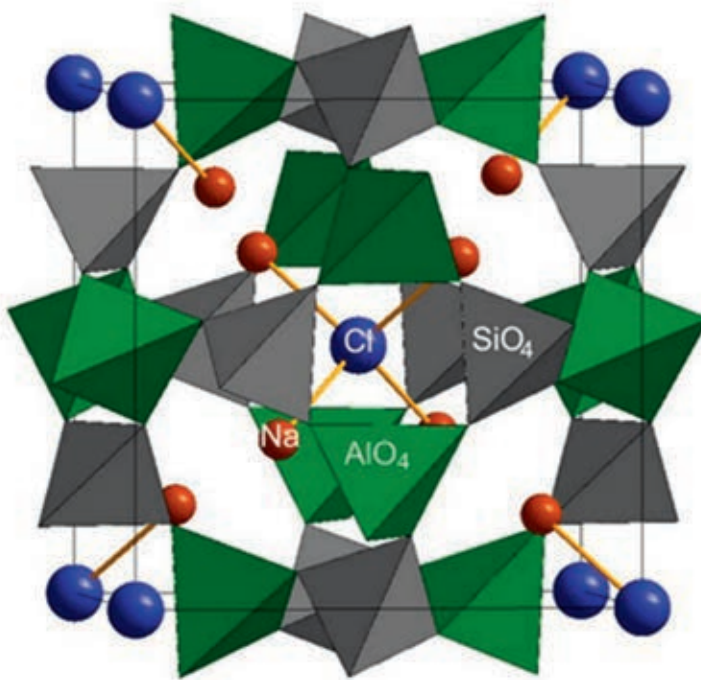
Figure 1 Hackmanite unit cell structure drawn from data in [18]. [V]

The literature is not in agreement on what the sulfur species in hackmanite actually is. It has been suggested that the form is one of the following: S_2^{2-}, S^{2-}, S_2^- SO_4^{2-} or SO_3^{2-} [10,15,19]. Also, the content of sulfur varies widely between samples and different locations. Peterson [15] reported sulfur contents for hackmanite samples obtained from Quebec, Canada to be between 0.05 and 0.30 mass-%, whereas Cano *et al.* [14] found SO_2 content of natural hackmanite from Brazil to be below the detection limit of XRF, *i.e.* less than 0.01 mass-%.

The natural hackmanite is known for its photochromic property. It has been first noted in 1834 by Robert Allan [5]. Blue, reddish and/or yellow luminescence has also been reported from natural hackmanites in multiple publications (*e.g.* [1,3,20–22]). The color and intensity of photochromism and luminescence vary between different locations and also between different samples from the same location. In addition to this, also the chemical compositions of different samples

obtained from different locations vary a lot [5]. This indicates that the chemical environment within the hackmanite material affects the optical properties.

2.2. Theory of luminescence

Luminescence, the emission of light from a material after it has been excited with external energy, is a term used to describe both fluorescence and phosphorescence. Both organic and inorganic materials can exhibit luminescence. Since the theory and terminology differs between these two, this review focuses only on inorganic materials. Still, it is important to note that also many organic compounds have luminescent properties.

By definition, fluorescence is light emission from allowed transitions, whereas phosphorescence results from forbidden transitions. Allowed transitions happen between states with the same spin whereas forbidden transitions are transitions between states with the same parity (*e.g.* all *d-d* transitions). [23] Whether a transition is allowed or forbidden affects the lifetime of the emission, i.e. allowed transitions give short luminescence and forbidden transitions give longer emission lifetimes. In inorganic materials, the electronic states participating in the luminescence process are seldom pure states. Thus, it is difficult to define whether an emission is actually fluorescence or phosphorescence. However, it is common in the literature that all short-lived emission is called fluorescence and all long-lived emission is phosphorescence, even if this is not strictly true. All solid luminescent materials are called phosphors, which comes from Greek, meaning *light bearer* [24].

Like with many phenomena, the different types of luminescence have different names and sometimes they have different meanings. In this work, PL is used to describe short, photon induced luminescence that emits during the excitation. In literature this sometimes falls under fluorescence. Persistent luminescence (PeL) is used for the longer emission that is visible for minutes after the excitation source has been removed. In the literature, phosphorescence is sometimes used to describe the latter phenomenon.

The first human made luminescent material is the Bologna stone from 1602 that was prepared by an alchemist Vincentinus Casciarolo. He heated barite ($BaSO_4$) and it resulted in barium sulfide (BaS) that would glow orange/red light after the exposure to the sun. The impurities present in both the barite and the charcoal used in the heating are held responsible for the luminescence, according to the knowledge today. Since the light emission continues a long time after the excitation the material exhibits persistent luminescence. [24–26]

Luminescence occurs inside a host material, within or around an activator. The activator is usually an impurity, vacancy or other defect inside the host crystal that somehow disturbs the otherwise organized structure of the host lattice. The activator absorbs the excitation energy and gets excited forming a luminescent center alone or together with the surrounding atoms from the host lattice. The excited state then relaxes and returns back to the ground state. The return can be radiative or non-radiative (*i.e.* host lattice vibrations). If the return is radiative, luminescence is obtained (**Figure 2**). [24,27]
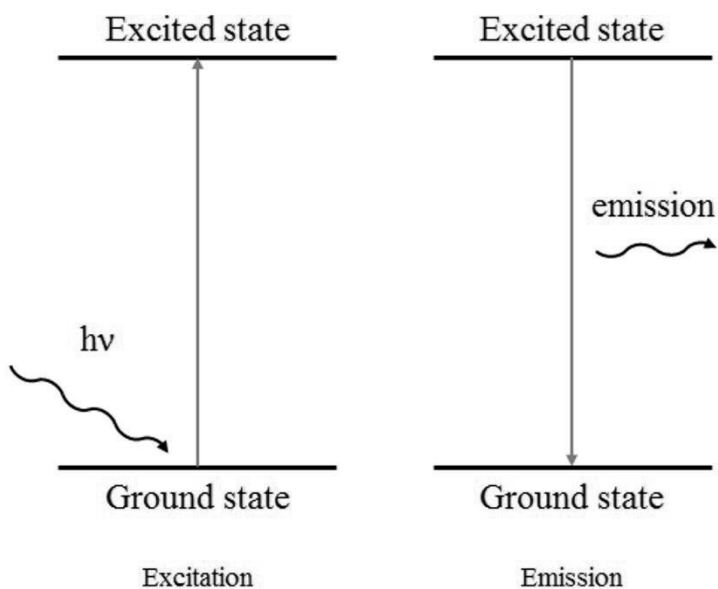
**Figure 2** Schematic overview of luminescence phenomena.

In some cases, the activator can not be directly excited. In this case, another ion can absorb the energy and transfer it to the activator. This other ion is called a sensitizer. In this, more complex luminescence mechanism, the sensitizer gets excited, then the energy transfers non-radiatively to the activator. When the excited state of the activator then relaxes, the radiative return emits luminescence [27]. The mechanism and application of different types of luminescence are looked into in more detail in the following sections (2.2.1–2.2.3).

2.2.1. Photoluminescence

PL emission occurs during or directly after (within milliseconds) the excitation. In **Figure 2** a simplified scenario is presented. In reality, the process is more complex and involves also the vibrational levels of the ground and excited state. Some of the energy gets always lost to vibrations, which is why the emission ($E = h\nu_2$) is of lower energy, *i.e.* higher wavelength than the excitation ($h\nu_1$). Thus, equation 1 applies to PL emission.

$$h\nu_1 > h\nu_2 \qquad\qquad \text{(Eq. 1)}$$

A more detailed description of the processes in PL is shown in **Figure 3**, but also this is somewhat simplified and does not consider *e.g.* the differences between the bonding in the ground and excited states that can be accounted for by using configurational coordinate diagrams [27]. First, the material absorbs a photon with the energy of $h\nu_1$. This energy lifts the system from the ground state to one of the vibrational states of the excited state. Here, the system quickly seeks the minimum energy position releasing some of its energy non-radiatively. From the lowest energy state of the excited state, the system then returns back to the ground state releasing a photon with the energy of $h\nu_2$. The times involved in PL are really short. The non-radiative relaxation happens in a time scale of 10^{13} s^{-1} and the emission lifetime is between ns and ms. [27]
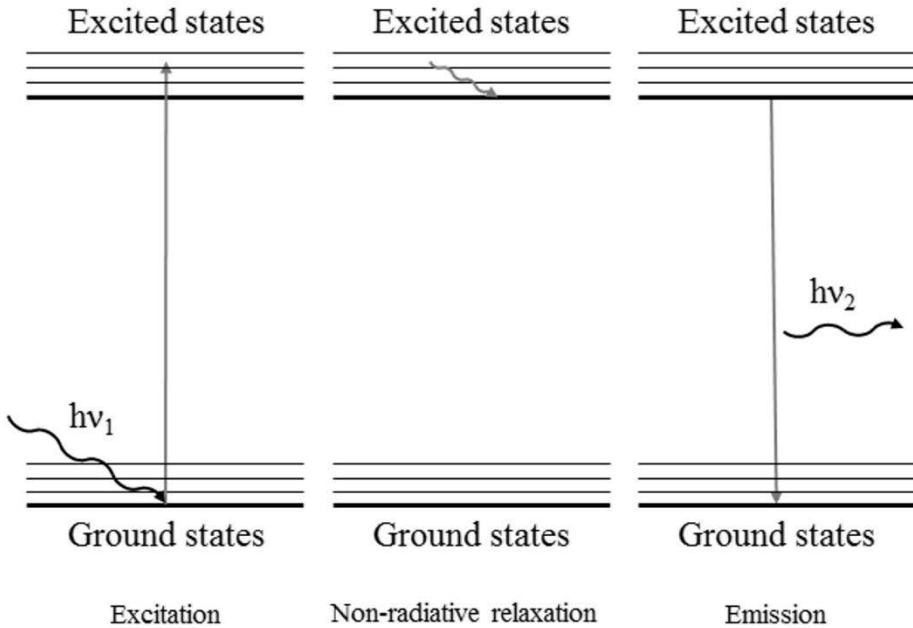
Figure 3 Simplified PL mechanism including vibrational states.

There are many possibilities for the activation ion in PL materials. Common activation ions include, for example, rare earth ions [28] and transition metal ions [29]. Rare earth ions have two different emission types. The first one is line emission that results in narrow, sharp lines in the emission spectra. This emission occurs from the $4f^n$ configuration of the ions. A couple of examples of these ions include Gd^{3+} ($4f^7$), Eu^{3+} ($4f^6$) and Tb^{3+} ($4f^8$). The other emission type in rare earth ions is band emission, where the emission band is wider. This emission happens when electrons return from a $5d$ orbital to the $4f$ orbital. This emission can be obtained from both trivalent (*e.g.* Ce^{3+} and Nd^{3+}) and divalent (*e.g.* Eu^{2+} and Yb^{2+}) ions. From transition metal activation ions, a couple of examples include Cr^{3+}, Mn^{4+}, Mn^{2+} and Fe^{3+} [29]. PL emission can also be obtained from alkali halides. In the case of alkali halides, the emission is exciton emission. Alkali halides have large band gaps and are thus transparent as pure crystals [30] but PL can still be observed from alkali halides doped with ns^2 ions [27,31]. In ns^2 the n represents the number of shells and s^2 represents the population on the

s-orbital. There is a large variety of such ions and they are shown in **Table 1** [30]. The exciton emission can be obtained from pure alkali halides, but with doping, the emission can be enhanced. For example, phosphors of thallium alkali halides have been extensively studied [32,33]. [27]

Table 1 ns^2 ions and their charge. [30]

n	Ion				
4	Cu^-	Zn^0	Ga^+	Ge^{2+}	As^{3+}
5	Ag^-	Cd^0	In^+	Sn^{2+}	Sb^{3+}
6	Au^-	Hg^0	Tl^+	Pb^{2+}	Bi^{3+}

PL is used in many applications, from which the most common is lighting and displays [34]. Light emitting diodes (LEDs) [35] and fluorescent lights used today are based on the PL induced in phosphor materials. PL has also other applications that do not show up in everyday life. A couple of examples of these applications include luminescence sensors [36] and luminescence thermometry [37].

2.2.2. Persistent luminescence

During the first years after the creation of the first manmade PeL material, the Bologna Stone, the research in persistent luminescence materials didn't advance much [38]. Only in the 1990s new, efficient PeL materials were created. This is also the time when different proposals for PeL mechanisms started to appear [25]. Long after this, only in 2012, the mystery of the Bologna stone was finally solved repeating the synthesis using materials obtained from Bologna and using modern methods to study its properties [26].

For a long time, ZnS was the best PeL material but in 1993 the real breakthrough was made when T. Matsuzawa *et al*. discovered the long and bright persistent luminescence of $SrAl_2O_4:Eu^{2+},Dy^{3+}$ [39]. The new phosphor met the needs of the time showing bright PeL for over 30 h with green emission extremely suitable for the sensitivity range of human eyes. The material could be excited with conventional lamps instead of UV that was needed before. In the consumer

point of view the best improvement was the fact that no radioactive elements were used to produce the PeL. Before this, radioactive elements like radium and promethium were used in PeL materials to obtain longer PeL durations. [38,39]

Currently, many efficient PeL materials based on lanthanide emission are available in the red, green and blue (RGB) colors (**Figure 4**). A couple of examples of these materials are $SrAl_2O_4:Eu^{2+},Dy^{3+}$ (green), [39] $CaAl_2O_4:Eu^{2+},Nd^{3+}$ (blue), [40] $Sr_2MgSi_2O_7:Eu^{2+},Dy^{3+}$ (blue) [41] and $Y_2O_2S:Eu^{3+},Mg^{2+},Ti^{4+}$ (red) [42]. The blue and green PeL materials are efficient with many commercial applications. The intensity and duration of the red PeL materials are considerably weaker compared to green and blue phosphors. Also, with all current materials, the problem arises from lanthanides that are expensive which makes the total costs for the materials higher. [38]
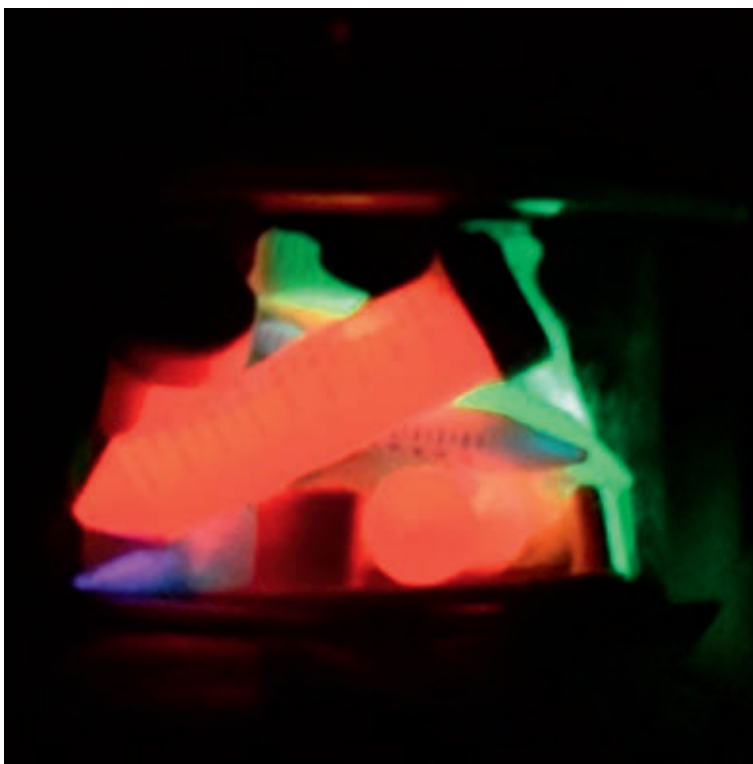
Figure 4 Synthetic PeL materials in RGB colors minutes after excitation with 254 nm.

When talking about PeL duration, the terms short and long are used somewhat arbitrarily. There has not been any set limits to quantify the time needed for PeL to be called long. In addition to this, PeL is usually measured in arbitrary units (a.u.) which is connected to the current spectrometer in use and can not be compared with other measurements made elsewhere. Also, measurement parameters such as the detector voltage used in the measurements affects the observed intensity. Xu and Tanabe show a typical example of this when measuring the light emission of a commercial LED with different photomultiplier tube (PMT) detector input voltages [38]. The signal varies between 1 and 12 600 000 µV depending on the detector voltage. Thus, a common unit is needed for PeL duration measurements. A good option is luminance, which is measured in mcd/m². There is a set value of 0.32 mcd/m² (corresponding to 100 times the perception limit of the human eye) that is commonly used as a limit when measuring luminance [43]. The time needed for the PeL material to reach this limit is considered to be the time that the luminescence can be seen with the naked human eye. Since the luminance measurement takes into account the human eye sensitivity to light, it is thus a good unit to use, when comparing materials used in applications viewed by people (for example exit signs and glow-in-the-dark toys).

It is not possible to give a general mechanism for PeL since the mechanism depends on the host lattice and active ions present. Because of this, only the basic principles are presented here. In PeL, two different centers are present: the emission center and the trap center. The emission center is usually either a lanthanide ion or a transition metal ion [44–46]. Trap centers are usually intentionally introduced co-dopants but they can also be minor impurities or lattice defects [40,47–49]. In general, the PeL process involves 4 steps: the excitation, trapping, detrapping and recombination. A schematic overview of the processes is shown in **Figure 5**. [38]
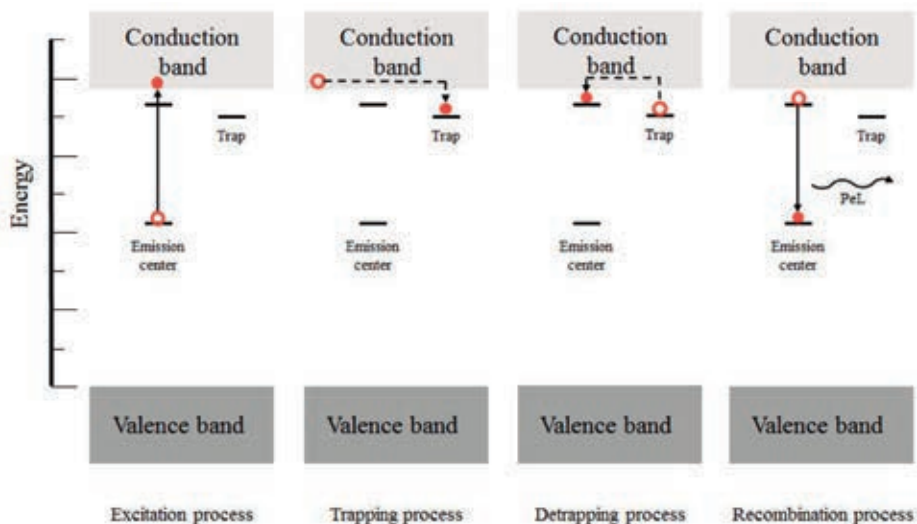
Figure 5 Excitation, trapping, detrapping and recombination processes involved in PeL as described in [38].

In the excitation process the external excitation energy lifts electrons from the ground state of the emitting center to conduction band. The energy needed for the excitation depends on both the band gap and the position of the emission center's ground state with respect to the conduction band and is thus characteristic for the host lattice – emission center combination. In the trapping process the electrons in the conduction band are non-radiatively captured by traps located close to the bottom of the conduction band. When the electrons are then thermally stimulated to leave the traps, the detrapping process happens. This suggests that the depth and density of the traps affects the duration and intensity of PeL. Lastly the electrons travel back to the emission center. There the recombination of the electron–hole pair happens yielding delayed emission characteristic for the emission center. [38,50]

The research of PeL phosphors has advanced in the years after its discovery and today PeL materials are in use in many applications, for example self-lit exit signs, [51] glow-in-the-dark toys [52] and some medical and diagnostic applications [53–55]. The challenges with PeL phosphors still remain with red and white emitting materials. While commercial red PeL phosphors are currently

in the market, the intensity and duration of green and blue phosphors is far superior compared to the red ones. As with the white PeL phosphors, some are listed in refs. [38,56] and in **Table 2**. The duration of PeL in these phosphors varies from minutes to a couple of hours with the limit of 0.32 mcd/m^2 [57–62]. Another possibility to obtain white PeL could be to combine the RGB colors. With this approach the different intensities and lifetimes of different phosphors would highlight and the color would soon shift away from white, especially because the short lifetimes of red PeL phosphors. The red and white PeL phosphors will thus stay in the research interest of scientists.

Table 2 White PeL materials presented in refs [38] and [56].

Host material	Activator	Host material	Activator
$CaMgSi_2O_6$	Dy^{3+}	$SrSiO_3$	Dy^{3+}
$CaSnO_3$	Pr^{3+}	$Sr_2Al_2SiO_7$	$Ce^{3+} \rightarrow Dy^{3+}$
$CaZnGe_2O_6$	Dy^{3+}	$Sr_3Al_2O_5C_{12}$	Eu^{2+}
$CdSiO_3$	Dy^{3+}	$ZbGa_2O_4$	defects

2.2.3. Up-conversion luminescence

Up-conversion luminescence is a rare case of luminescence, where the emitted photon has a higher energy than the excitation photon. This is achieved by stacking of low energy photons. Different routes for the stacking have been suggested and the energy levels of the sensitizer and the activator ion determine which route is used. If the activator ion has multiple energy levels capable of absorbing energy, the mechanism can be APTE or 2-steps absorption. If there are not suitable energy levels for this kind of absorption, the co-operative mechanisms or second harmonic generation can happen, to enable the luminescence. All the different mechanisms are presented in **Figure 6**. [63]
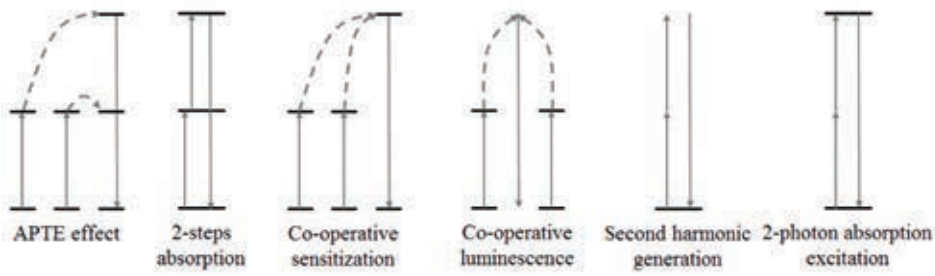
Figure 6 Different mechanisms for up-conversion luminescence. [63]

Trivalent lanthanides are usually used in up-conversion luminescence, since they have multiple energy levels suitable for absorption and emission [64]. A common pair of sensitizer and activator ions is ytterbium and erbium. The up-conversion luminescence obtained from materials containing these ions is based on the energy transfer up-conversion, also called APTE [63]. In this mechanism, two ytterbium sensitizers absorb the infrared (IR) excitation. Then, they transfer the excitation energy to an erbium ion located nearby. The energy levels of erbium allow the stacking of the two photons and when the excitation then relaxes, red and green luminescence are observed (**Figure 7**).
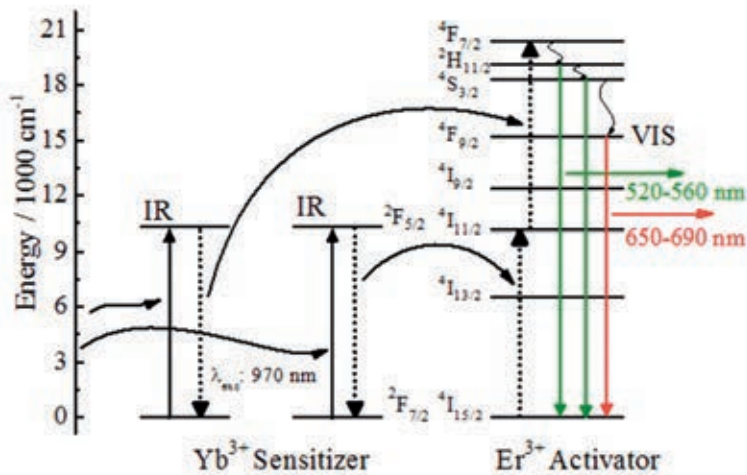
Figure 7 Energy transfer up-conversion mechanism with ytterbium and erbium ions. [V]

Up-conversion luminescence can be used, for example in solar cell applications, [65] in pH sensors [66] and in biological detection [67]. The advantage of up-conversion materials is that when IR excitation is used, there is no auto fluorescence in biological medium at the visible wavelengths, where the up-conversion emission is detected. The drawback is that the up-conversion process is so weak that a strong excitation source (typically a laser) is needed to induce visible emission.

2.3. Photochromic materials

Photochromism is a phenomenon where coloration of a material is reversibly induced with a photon [11,68]. The phenomenon is sometimes also referred to as tenebrescence, especially among mineralogists. The two are thus the same phenomena.

Both organic and inorganic materials exhibit photochromism. In organic materials, the color transformation is induced by breaking and reforming bonds, [69] whereas in inorganic materials, the photochromism is induced by the formation of F centers [70]. The F center, also known as color center, is an anionic vacancy in the material which has been filled with an electron. When the trapped electron then absorbs light, the color of the material changes. This review is again going to focus only in the photochromism observed in inorganic materials.

In inorganic materials, photochromism is observed for example in alkali halides, [70] silver halides, [71] alkaline earth fluorides, [72] many minerals [73] and in titanium dioxide [74]. The photochromic materials where the coloration is induced with UV radiation and the discoloration with ambient light, are the most studied ones. [11]

The mechanism for photochromism is always related to the material in which it happens. The host material and its dopants and defects all play a role in the mechanism. Medved [70] proposed a mechanism for color center formation in 1954 for hackmanite and sodalite. This mechanism is now used as an example to better understand the processes involved in photochromism.

The mechanism is presented in **Figure 8**, where the F and U levels between valence band and conduction band represent normal defects in material and dopant or impurity levels, respectively. In the photochromism mechanism, there are 4 different processes. The first process (1) happens when electrons located in the U energy levels absorb UV radiation and raise to the conduction band. After this, processes 2 and 3 compete. In the process 2 the electrons get trapped to empty F energy levels forming color centers. In the process 3, the electron returns back to U energy levels possibly releasing luminescence emission. If color centers are formed (process 2), the color of the material changes. After this, if the color center absorbs a suitable amount of energy that can raise the electron back to the conduction band (process 4), the processes 2 and 3 compete again. Since some electrons always relax via process 3, in time all the color centers will have been discharged and the material has returned back to its original color. Since the discoloration needs some energy, that is usually received from light or heat, if the material is kept in dark in room temperature, the color centers can not discharge and the colored form stays permanently [10]. [70]
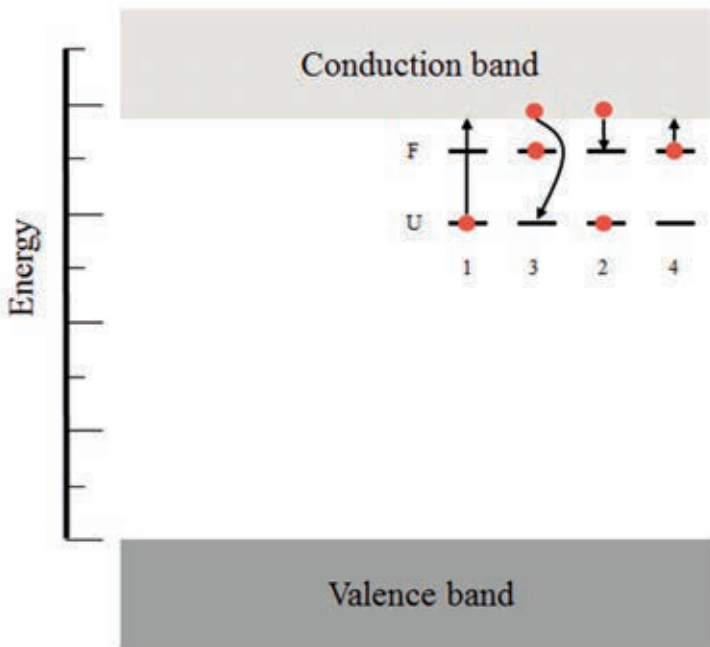
Figure 8 Processes 1-4 involved in photochromism mechanism in sodalites according to [70].

Photochromic materials are already in use in many applications and they are also studied for some interesting new application areas. Some application areas for photochromic materials are optical memories, [68,75] optical switches, [68,76] jewelry, [10] colorable eyeglasses [77] and even fabrics [78]. Some more recent possible applications for photochromic materials are focused on UV detection [79].

2.4. Optical properties of hackmanites

Natural hackmanites have been reported to show photochromism and sometimes also PL [5,20,21] (**Figure 9**). In synthetic hackmanites, photochromism and PL are usually present [7,9,80]. The photochromism in natural hackmanites is usually visible when the mineral is first mined and after this, the coloration disappears when the mineral is exposed to natural light [81,82]. In addition to this, some of the natural hackmanites obtain the purple color, when kept in the dark [5].

**Figure 9** A photograph of a rock containing natural hackmanite mineral in its colored form.

In 1936 Lee discovered, that the pink color of a natural hackmanite could also be induced using UV radiation and reversibly erased with an electric lamp [20]. Some years later Medved prepared synthetic hackmanites and observed a similar coloration with an absorption maximum around 530 nm, when exciting with

x-rays but only after using a reducing atmosphere in the synthesis, was he able to prepare synthetic hackmanite with photochromism excitable with UV radiation [7].

In 1969 Williams *et al.* studied the photochromism in hackmanites and found out that the partial substitution of Cl with other halogens speeds up or slows down the coloring rate in synthetic hackmanites, depending on the electronegativity of the halogen. The absorption maximum, *i.e.* the color of the material could also be shifted from 530 to 510 nm, when fluoride was added. [8]

The structural changes happening during color center formation in synthetic hackmanites have also been studied. The research shows that when a color center is formed, the atomic distances between sodium and oxygen increase and the distance between sodium and chloride decreases. This results in an expansion in the lattice parameter indicating that the hackmanite framework bends during the formation of a color center. When the hackmanite is then bleached, the parameters return back to their original values indicating reversible bending. [10]

Gaft *et al.* have studied the laser-induced luminescence in natural hackmanites obtained from Russia and Afghanistan. The natural hackmanites exhibited red and violet-blue luminescence under short UV excitation resulting from Fe^{3+} or Cr^{3+} and mercury type s^2 centers, respectively (**Figure 10**). Under 355 nm excitation, yellow-orange luminescence from S_2^- was observed. The results concluded that the emission of natural hackmanites is not resulting from only one luminescence center, but several luminescence centers contribute to the emission. [3]
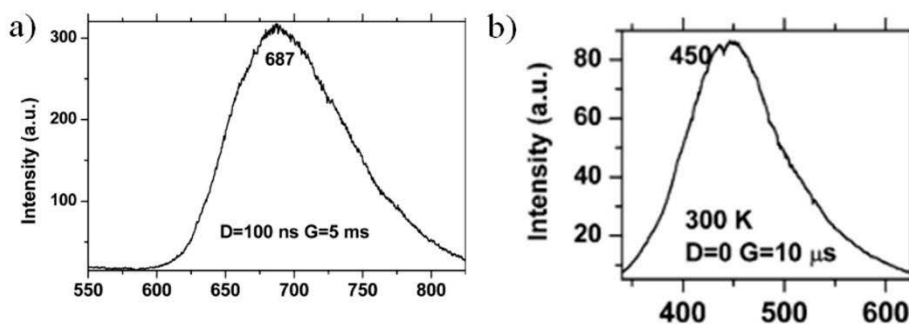
Figure 10 Time-resolved luminescence under 266 nm excitation at 300 K from a hackmanite obtained from a) Russia and b) Afghanistan. [3]

Also the luminescence in synthetic hackmanites has been studied. Kirk noted in his research that the luminescence is similar in natural and synthetic hackmanites and is not affected by the fact if the material is photochromic or not. Thus he concluded that the luminescence center is different than the color center in hackmanites. In this work Kirk assigned the luminescence to the polysulfide ion present in the material. [21]

Later, the effects of sulfur on the optical properties has been studied even more. Recently it was reported that the addition of extra sulfur into hackmanite structure destroys the photochromic property of the material and leaves it in a permanent blue or green state. This is probably caused by the concentration of the photoactive species S_2^- exceeding the threshold for the concentration quenching. This means that the excitation energy is released by radiation less decay instead of forming color centers. [12]

The natural hackmanite is commonly used as a jewelry because of its lovely color and the ability to change color, when in contact with UV (**Figure 11**). To date, no commercial applications are available for the synthetic hackmanites, even though the use of hackmanites in, for example, storage displays has been studied [83].

Figure 11 Natural hackmanite UV colorchange ring before and after excitation. Picture from etsy.com. [84]

2.5. Synthesis of sodalite materials

Hackmanite minerals can also be synthesized. Different methods have been suggested for the synthesis. The synthesis of hackmanite is usually the same as for common sodalite, only sulfur is added. High temperatures and long reaction times are a common factor in most of the methods.

In sodalite synthesis regardless of the synthesis method, starting materials usually include zeolite or other Si and Al containing precursors and NaCl. The starting materials can vary depending on the desired stoichiometry of the end product. When preparing hackmanites, a source for sulfur is also needed. For this, Na_2SO_4 is usually used.

2.5.1. Solid state synthesis

The most common synthesis method used for sodalite preparation is the solid state synthesis. In this method, the solid starting materials are ground together and heated at high temperatures in two steps, in air and in a reducing atmosphere. The

order of these steps can be reversed and both methods have been used in the literature before.

For example, Kirk *et al.* have used a method that first reduces the sample, prepared from oxides forming $NaAlSiO_4$ and $NaCl + Na_2SO_4$, at 900 °C under hydrogen atmosphere. After this, the sample is heated for 15 min under air, again at 900 °C to oxidize some of the sulfur in the hackmanite material. The hackmanites prepared in this way showed orange-yellow luminescence and had efficient, reversible photochromic properties. [21]

On the other hand, Armstrong *et al.* used a solid state synthesis with reverse order to produce photochromic hackmanite, though there is no mention about luminescence. In this synthesis, the ground mixture of Zeolite A, NaCl (or NaBr) and Na_2SO_4 is first heated at 850 °C under air for 48 h. After cooling down the material is re-ground and then heated in H_2/N_2 (5%/95%) atmosphere for 2 h. The synthesis also includes a washing step with distilled water to remove excess sodium starting materials. [10]

Exceptionally, Medved has been able to prepare sodalites with a solid state reaction in just one step. In this synthesis, Al_2O_3, SiO_2, NaOH and NaCl were mixed in a mortar and ball milled. The mixture was then placed into a clod oven in a platinum crucible. The temperature of the oven was then raised to 1060 °C and kept there for 24–72 h. The materials prepared this way showed photochromism under x-ray excitation. [70]

With solid state synthesis, pure sodalite phase is usually achieved after washing the excess starting materials away. Since the temperatures are high and reaction time is long, the obtained materials are microcrystalline in size. To produce nanosized sodalite, different methods are needed.

2.5.2. Hydrothermal synthesis

Hydrothermal synthesis is one way to prepare nanosized sodalite. This method also allows the preparation of sodalite at considerably lower temperatures.

In the synthesis introduced by Mikuła *et al.*, aluminate solution and silicate solution (**Table 3**) are mixed together at 95 °C while first shaking for 5 min and then allowing them to crystallize for 24 h without stirring. The materials were then washed and dried to reach pH 7. [85]

Table 3 Chemicals and amounts needed to prepare aluminate and silica solutions used in ref [85].

Aluminate solution		Silica solution	
Chemical	**Amount**	**Chemical**	**Amount**
Sodium hydroxide	40.0 g	Sodium hydroxide	60.0 g
Aluminum hydroxide	15.6 g	Sodium chloride	87.6 g
Deionized water	200 ml	Deionized water	318 ml
		Aerosil	18 g

Another hydrothermal synthesis uses autoclaves to achieve higher pressures for the synthesis. In this method starting materials (SiO_2, Al_2O_3, NaOH, NaCl and Na_2SO_4) are thoroughly mixed in water at 100 °C in an open beaker. Then, the mixture is transferred to an autoclave and heated at 200–400 °C for 12–48 h. The pressure is between 13700–27600 kPa. After the synthesis the product is filtered and washed. The synthesis produces sodalite, but to obtain photochromism in the material, a third step is needed. In this step, the product is heated at 900 °C for a maximum of 30 min in an inert or a reducing atmosphere. [8]

Chong *et al.* used also a hydrothermal synthesis to prepare iodosodalites. They used NaI, $NaAlO_2$ and SiO_2 as starting materials together with NaOH as a mineralizing agent. The starting materials were dissolved in water and NaOH was dissolved separately. Then the solutions were mixed and heated in an autoclave. The time varied between 1 and 20 days and the temperature varied between 100 and 200 °C. The results indicate that the optimal temperature for this synthesis is between 140 and 180 °C. [86]

Hydrothermal synthesis offers a good way to prepare sodalite in lower temperatures. Still, synthesis times varying between 12 and 120 h [8,85,87] make the hydrothermal synthesis as time consuming as the solid state synthesis.

2.5.3. Solution synthesis

A solution synthesis can also be used to prepare sodalite materials. In this method used by Johnson *et al.* to produce Ga and Ge sodalites, stoichiometric amounts of framework precursors (Na_2GeO_3, $NaGaO_2$, $NaAlO_2$ and $Na_2SiO_3 \cdot 5 H_2O$) are refluxed together with a salt that is to be incorporated in the cavities. The water mixture is refluxed for 24 h at 120 °C. To stabilize the anions in the mixture, some base can be added. [88]

The solution synthesis is similar to hydrothermal synthesis but it can be done in ambient pressure enabling the synthesis without any special equipment. The preparation times needed for this synthesis are also considerably shorter than the 2–20 days needed in some of the previously introduced synthesis methods.

2.5.4. Microwave synthesis

Microwave (MW) synthesis offers a fast and efficient synthesis method for sodalite production. It produces good quality samples with less energy, since the preparation times are short.

In a MW synthesis, stoichiometric amounts of framework precursors ($NaAlO_2$, Na_2GeO_3 and $Na_2SiO_3 \cdot 5 H_2O$ in case of Johnson *et al.*) are mixed in water with a salt that is to be incorporated in the cavities. The synthesis can be performed in a domestic microwave oven using a microwave digestion bomb inside. At 1000 W the synthesis can be performed in only 10 s, but 20 s synthesis produces the best crystallinity in the samples. The method works well on Ge containing sodalites, but aluminosilicate sodalites produced this way had poor crystallinity. Also, since the pressure and temperature can not be regulated properly in this method, damage to the autoclave is possible. [88]

Another type of MW synthesis is the microwave-assisted structure-conversion method proposed recently, to produce photochromic hackmanites in just one 12–20 min step [89]. In this kind of synthesis, Zeolite A is used as a starting material for the hackmanite since it has a similar structure with Si- and Al-cages with the correct Si/Al ratio. In this method, Zeolite A and other starting materials are mixed and exposed to MWs with activated carbon surrounding the sample holder. The activated carbon acts as a susceptor, absorbing the MWs and generating heat and a reducing atmosphere (**Figure 12**). With 400 W power and 12–20 min reaction time, a temperature of around 829 °C is achieved. This temperature is enough to convert the structure of Zeolite A together with NaCl and sulfur to hackmanite.
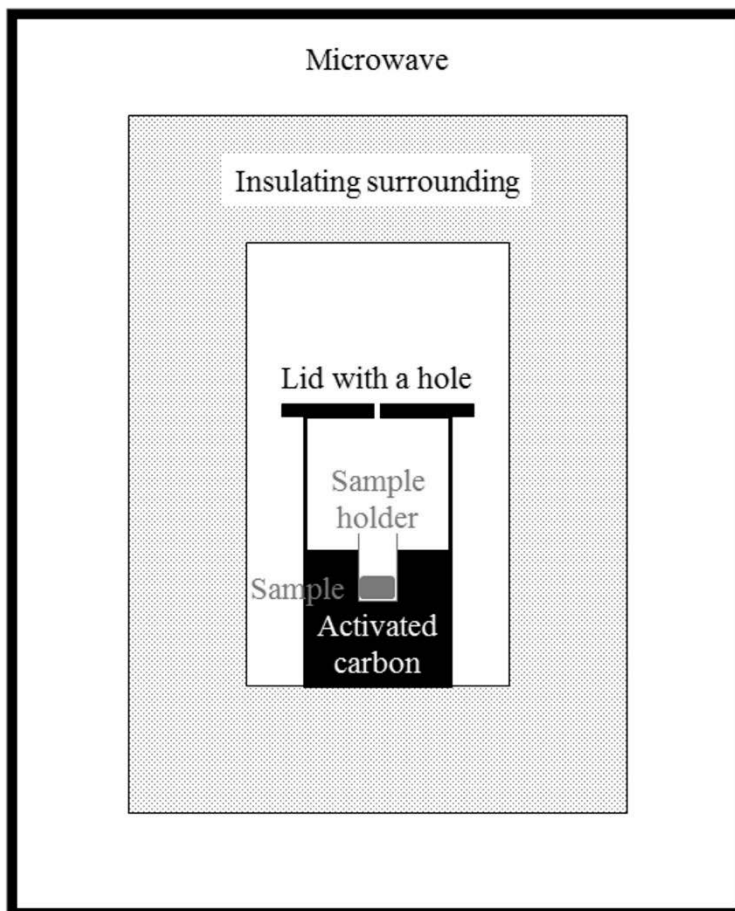
Figure 12 A Cross-section of a setup used in a MW synthesis.

3. Aims of the experimental work

The aim of this work was to study synthetic hackmanite minerals and their properties (photoluminescence, persistent luminescence, photochromism and up-conversion luminescence). The research was conducted using different spectroscopic methods on synthesized hackmanite materials. The main research topics were the following:

1. Understanding the mechanisms of the optical properties of synthetic hackmanites (I–IV).

2. Improving the brightness and duration of photoluminescence and persistent luminescence in synthetic hackmanites (I and III).

3. Controlling the photochromism in synthetic hackmanites (II and IV).

4. Preparing a synthetic hackmanite material with multiple different optical properties suitable for optical multiplexing (V).

4. Materials and methods

4.1. Materials preparation

Synthetic hackmanites were prepared using a solid state synthesis [10]. The basic components for hackmanite synthesis were 0.7 g of Zeolite A (dried for 1 h at 500 °C), 0.24 g of NaCl and 0.06 g of Na_2SO_4. The starting materials were first ground in a mortar for 20 min. When thoroughly mixed, the starting materials were transferred to a ceramic alumina crucible and heated in a Lenton furnaces TLF 1400 tube furnace in a static air atmosphere for 48 h. After the heating the furnace was let to cool down freely to room temperature.

After cooling down, the samples were again ground in a mortar for 10 min and then they were transferred to the crucibles and heated in a flowing H_2/N_2 atmosphere (10%/90%) inside a glass reactor in a Thermo-Lindberg/blue M tube furnace. The furnace was heated for 45 min to acquire the desired temperature of 850 °C and the temperature was held stable for 2 h. After this the furnace was let to freely cool down and the gas flow was turned off once the temperature had reached temperatures below 150 °C. Finally, the samples were ground to achieve a more uniform structure throughout the sample.

Some samples were also washed after synthesis to remove the non-reacted starting materials. The samples were washed with about 1 ml of quartz distilled water per 200 mg of sample. The samples were then centrifuged for 10 min at 5000 g. After this, the excess water was removed and the samples were dried in a desiccator usually overnight. [I-V]

4.1.1. Finding the optimal S/Cl composition for hackmanites

The precursor amounts of 0.7 g Zeolite A, 0.24 g of NaCl and 0.06 g of Na_2SO_4 were used as a starting point for the research as described by Armstrong *et al.* [10]. The optimal concentration for Cl and S in $Na_8(AlSiO_4)_6(Cl_{2-2x-0.2}S_x\square_{0.2})$ was tested, while the vacancy concentration was kept constant at 0.2. During these tests five different ratios of NaCl and Na_2SO_4 were used during the synthesis. The amounts used are listed in **Table 4**. The synthesis was carried out as described in chapter 4.1 with all NaCl and Na_2SO_4 amounts.

Table 4. Amounts of NaCl and Na_2SO_4 used in synthetic hackmanite synthesis and the resulted n(S):n(Cl) ratios [I].

NaCl (g)	Na₂SO₄ (g)	n(S):n(Cl)
0.2727	0.0000	0.00
0.2400	0.0600	0.06
0.2121	0.1200	0.13
0.1818	0.1800	0.26
0.1515	0.2400	0.37

4.1.2. Doping synthetic hackmanites

When preparing synthetic hackmanites doped with different ions the dopant was added to the hackmanite starting material mixture usually as an oxide. The amounts were calculated in mol-% compared to NaCl and the equivalent molar amount of NaCl was then deducted from the mixture. Different dopant ions used in the syntheses are listed in **Table 5**.

After adding the dopants to the mixture, the hackmanite synthesis was carried out as described in the chapter 4.1.

Table 5. Different dopants used in the hackmanite syntheses and their molar amounts.

Dopant	Amount (mol-%)	Dopant	Amount (mol-%)
TiO_2	2	MnO_2	2
Yb_2O_3	3	Er_2O_3	1
	6		2
	9		3
	20		6
$YbCl_3 \cdot 6\,H_2O$	6	$ErCl_3 \cdot 6\,H_2O$	2
	20		6

4.1.3. Exchanging the alkali metal cation in synthetic hackmanites

When preparing synthetic hackmanites, the Na cation was sometimes partly replaced with Li, K or Rb. This was done by replacing some or all of NaCl in the synthesis with different chlorides. The total molar amount for all chlorides was kept constant during different synthesis.

After replacing NaCl partly or totally with different chlorides the hackmanite synthesis was carried out as described in the chapter 4.1.

4.1.4. Adding a flux to hackmanite synthesis

To make PeL last longer in synthetic hackmanites a small amount of boric acid (H_3BO_3) was added to the synthesis. Different amounts from 2.5 to 20 mass-% were tested. The boric acid was added to the starting mixture with the rest of the chemicals and the synthesis was carried out as described in the chapter 4.1

4.2. Characterization methods

To verify the structure and to compare the properties of the produced hackmanite samples different characterization methods were used.

4.2.1. Methods studying the structure

The structure and purity of the synthesized materials was checked using XPD measurements. The XPD results in the diffraction pattern of the studied material which can then be compared to existing reference patterns to confirm the crystal structure of the material. Hackmanite reference pattern [90] was used to confirm the right material was obtained. The XPD results can also be used to determine crystalline impurities within the sample material when comparing the resulting reflections to patterns for starting materials as well as other possible impurities [91]. The XPD patterns were recorded for 20 min using a Huber G670 detector with Cu $K_{\alpha 1}$ radiation at $\lambda=1.54060$ Å. The sample holder was shaken horizontally during the measurement to minimize the effect of preferred orientation.

From the obtained XPD data, unit cell volumes and interatomic distances were calculated with Rietveld analysis [92] using the FullProf program [93–95]. The Rietveld analysis uses the reflection positions and intensities to optimise the positions for atoms inside the unit cell.

For more detailed information about the impurities and dopant concentrations in the prepared samples, XRF measurements were carried out using a PANalytical Epsilon1 apparatus. The contents of elements heavier than sodium were tested with a 1 h measurement program. The spectra were compared against the internal Omnian calibration. The X-ray source in the apparatus was an Ag anode X-ray tube.

The impurities in hackmanite samples were investigated using inductively coupled plasma-mass spectrometry (ICP-MS). A PerkinElmer 6100 DRC apparatus was used for the measurements. The results gave the ppm amounts of impurities present in the material.

Particle sizes and stability in water was studied using transmission electron microscopy (TEM). The images were obtained with a JEM-1400 Plus apparatus.

The same apparatus was also used to obtain electron diffraction patterns. ImageJ program [96] was used to calculate the reflection d-spacings.

X-ray photoelectron spectroscopy (XPS) was used to study the valence of selected elements in the hackmanite materials. The measurements were carried out using PerkinElmer PHI 5400 spectrometer and the analysis of the results was conducted with CasaXPS software version 2.3.16 [97]. The X-ray source used was Mg K_α. A hemispherical electron energy analyzer was used as well as a neutralizer with a constant electron flux. To study the structural changes happening after excitation, some measurements were conducted after first exciting the material with 254 nm hand-held UVP UVGL-25 UV lamp for 30 min.

Scanning electron microscopy - energy-dispersive X-ray spectroscopy (SEM-EDS) was used to study the elemental distribution in sample grains. The method used a Leo 1530 Gemini microscope and a Thermo Scientific UltraDry SDD EDS-system. The microscope images were used for example to confirm the even distribution of dopant ions in the samples.

Magic angle spinning (MAS) NMR measurements were used to study the local structures in the solid samples. ^{23}Na, ^{27}Al and ^{35}Cl measurements were carried out for various samples to compare the environment around these elements in different samples. From minor differences in the resulting spectra, conclusions were drawn from the structure changes to induce different optical properties in the samples. The NMR apparatus used was a Bruker AV400 and the spinning rate used was 12 000 Hz or 10 000 Hz. Relaxation time was 0.1 s in all measurements. The ppm scale for ^{23}Na, ^{27}Al and ^{35}Cl measurements was calibrated against 0.1 molar NaCl in D_2O, 1.1 molar aqueous $Al(NO_3)_3$ and 1 molar aqueous NaCl respectively. To examine the radiation induced changes in the local structure, some samples were irradiated *ex situ* (30 min with a 254 nm 4 W UVGL-25 UV lamp) before the measurement.

Electron paramagnetic resonance (EPR) spectra were used to study unpaired electrons in the materials. The measurements were carried out using either a

Bruker ELEXSYS E500 X band EPR spectrometer or a homemade X band EPR spectrometer. The Bruker apparatus was equipped with a SuperX EPR049 microwave bridge and a SHQ4122 resonator. In the measurements, a frequency of ca. 9.0, 9.3 or 9.8 GHz was used. The microwave power was 5 mW for the Bruker apparatus and ca. 1 mW for the homemade apparatus and the modulation amplitude in the Bruker apparatus was 3 G whereas in the homemade apparatus a modulation field of 100 kHz was used. Measurements were carried out at temperatures ranging from 15 K to room temperature. An Oxford instruments cryostat and an ITC-4 temperature controller were used to monitor the temperature. In addition to measuring pristine samples, some samples were irradiated *in situ* (4 min with a 355 nm Nd:YAG laser) or *ex situ* (10–30 min with a 254 nm 4 W UVGL-25 UV lamp) to examine the changes the radiation induces in the electronic structure.

The local structures and bonds in the material were studied using Fourier-transform infrared (FTIR) spectroscopy. A Nicolet Nexus FTIR ESP spectrometer was used with a 4 cm^{-1} resolution. Each spectrum was measured between 400 and 4000 cm^{-1} from samples mixed with KBr in transparent disks. The disk preparation used a ball mill and a vacuum press. The measurements were carried out for selected samples before and after excitation with a 254 nm and 365 nm 4 W UVGL-25 UV lamp.

4.2.2. Methods studying the luminescence properties

When measuring the PL properties of the synthesized hackmanite materials, a Varian Cary Eclipse Fluorescence spectrophotometer was used. The spectrophotometer is equipped with a Hamamatsu R928 photomultiplier tube and a 15 W xenon lamp. The measurements were done from powder samples in a sample holder located at a 135° angle against the excitation radiation. The detector is located at a 90° angle against the excitation source. The parameters for the PL measurements using phosphorescence mode are listed in **Table 6**. The PL spectrum was usually recorded with 254, 310 and 365 nm excitation.

Table 6 Fixed parameters used in the Varian Cary Eclipse Fluorescence spectrophotometer for luminescence measurements.

| Parameter	Value	Parameter	Value
Total decay time	0.005 s	Excitation slit	10 nm
Number of flashes	1	Emission slit	2.5 nm
Delay time	0.1 ms	Data interval	0.2 nm
Gate time	5 ms	Detector voltage	800 V
Averaging time	0.005 s		

To observe the best excitation wavelength for synthetic hackmanite PL, excitation spectra were recorded with the same Varian Cary Eclipse Fluorescence spectrophotometer using phosphorescence mode. The parameters used for luminescence spectra (**Table 6**) were also used for excitation spectra measurements. The excitation spectra were recorded at the emission maximum locating around 470 nm depending on the samples. In some cases, also other emission wavelengths were used to record the emission spectrum, for example 530 and 660 nm.

The Varian Cary Eclipse Fluorescence spectrophotometer was also used to record the PeL spectra. For this the Bio/Chemi-luminescence mode was used. When measuring PeL spectra, the powder sample was first irradiated with a hand-held UV lamp at either 254 or 365 nm for 30 min. The measurement was then carried out using parameters listed in **Table 7**. For basic PeL spectra, the luminescence was recorded 1 min after ceasing the excitation. When PeL decay curves were measured, the luminescence was automatically measured in set intervals (1 min or 30 min) until the intended measurement time was reached.

Table 7 Fixed parameters used in the Varian Cary Eclipse Fluorescence spectrophotometer for persistent luminescence measurements.

Parameter	Value
Measurement range	350–700 nm
Measurement time	4 s
Emission slit	20 nm
Data interval	1 nm
Averaging time	0.005 s
Detector voltage	800 V

Luminance measurements were carried out to determine the time needed for the materials' PeL to fade to the standard photopic limit of 0.3 mcd m^{-2} [98]. The apparatus used was a Hagner ERP-105 luminance photometer connected to a computer via a volt-ohm-milliammeter (VOM) (**Figure 13**). Before the measurement the samples were excited for 30 min with a UVM-57 6 W 302 nm hand-held UV lamp. During the measurement the data was recorded every second for at least 3 h. If the time needed to reach the 0.3 mcd m^{-2} limit exceeded 3h, it was extrapolated from the collected results.

| Sample holder and detector | Luminance photometer | VOM | Computer |
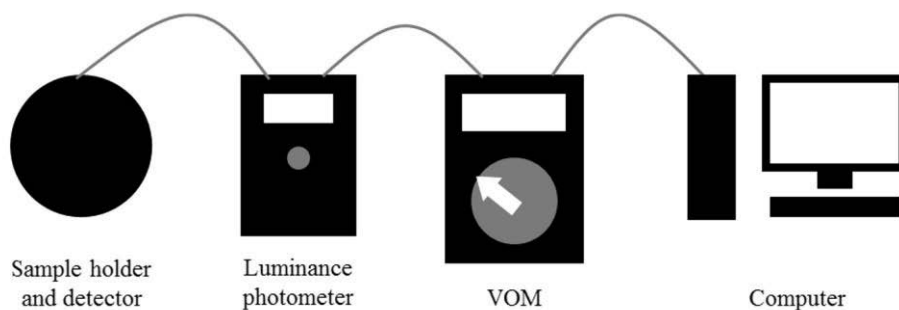
Figure 13 Schematic overview of the luminance measurement setup including the sample holder and detector, luminance photometer, volt-ohm-milliammeter (VOM) and the computer to record the data from the measurement.

TL measurements were carried out to further investigate the PeL properties of the materials. The equipment used was a MikroLab Thremoluminescent Materials

Laboratory Reader RA'04. The measurements were carried out using a 10 °C s^{-1} heating rate. The samples were irradiated prior to the measurement for 5 min using one of the following excitation courses: 4 W UVGL-25 UV lamp at 254 or 365 nm, LOT/QD LS0500 solar simulator lamp at 1000 W m^{-2}, Osram Dulux S 11 W fluorescent lamp, or Airam 9 W white LED lamp. The delay between excitation and measurement was 1 min. In some cases the sample was first preheated to a selected temperature and after that the glow curve was recorded. All TL curves were corrected for thermal quenching of luminescence and the initial rise method [99,100] was used to analyze the data. The trap depths were calculated from TL data plotted as ln(I) versus 1/T using the following equation (the initial rise method):

$$I\,(T) = C \exp\,(-E_T/kT) \qquad\qquad (Eq\ 2)$$

where C represents a constant that includes the frequency factor *s* which is assumed not to be temperature dependent, E_T is the energy of the trap, k is the Boltzmann constant and T is temperature in Kelvin [100].

Up-conversion luminescence was measured from glass capillaries filled with powder sample using an Avantes AvaSpec HS-TEC detector connected to a computer, and a 972 nm Fiber-coupled NIR laser diode IFC-975-008-F. A filter was used before the sample to allow only IR excitation to enter the sample (Edmund optics, hot mirror). The measurements were carried out at room temperature at a 90° angle between the laser excitation and the detector (**Figure 14**). A short-pass filter (Newport 10SWF-850-B) with a cutoff of 850 nm was used after the sample to block excitation radiation from the detector. The sample was spun during the measurement. The integration time was 1 000 ms and 10 averaging measurements were done.
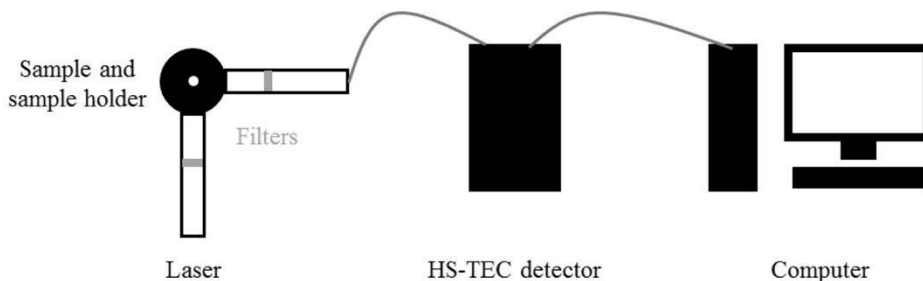
Figure 14 Schematic overview of the up-conversion luminescence measurement setup including laser, filters, sample holder, HS-TEC detector, and the computer to record the data from the measurement.

4.2.3. Methods studying the photochromic properties

The photochromic properties of synthetic hackmanites were studied using reflectance spectroscopy. This allows a quantitative comparison of the sample color induced by the excitation radiation. The reflectance spectra were collected under a 60 W incandescent light bulb with an Avantes AvaSpec 2048-14 spectrometer connected to a computer using 400 ms integration time and 30 averaging measurements (**Figure 15**). The reflectance of the samples was measured before and after excitation and the difference in the resulting spectra was used to measure the photochromism in the sample. For sample excitation a 254 nm 4 W hand-held UVP UVGL-25 UV lamp was used for 5 min.
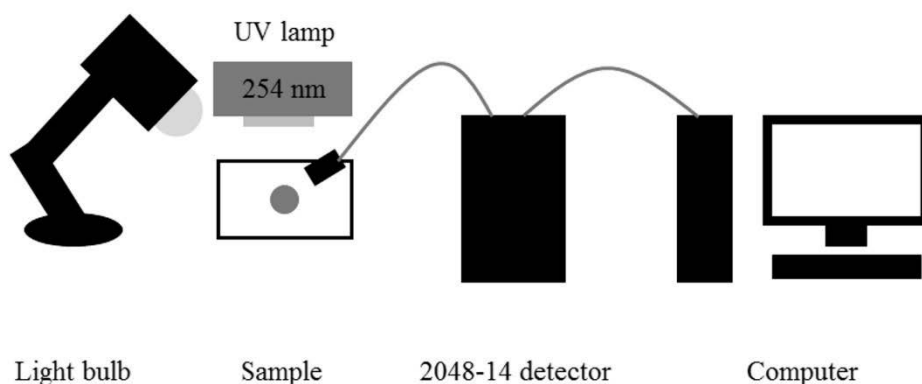
Figure 15 Schematic overview of the reflectance measurement setup including light bulb, UV lamp, sample, 2048-14 detector, and the computer to record the data from the measurement.

Sample coloring and discoloring wavelengths were also investigated to get the excitation spectra for photochromism. Reflectance spectroscopy with an Avantes AvaSpec 2048-14 spectrometer was also used to detect this. The samples were illuminated from 20 cm above with 60 W incandescent light bulb. The coloring in the samples was induced using a 30 min excitation with a 150 W Osram XBO 150W/4 xenon short-arc lamp with an Optometrics DMC1-01 monochromator. The discoloring by optical stimulation was studied by first coloring the sample for 5 min with a 254 nm 4 W hand-held UVP UVGL 25 UV lamp. Next, optical stimulation was given using the same xenon short-arc lamp and exposure time as described above for the coloration study.

To study the thermal discoloration of photochromism, a new method was developed called thermotenebrescence (TT). In the method, colored samples were exposed to rising temperature and their reflectance spectrum was measured as a function of temperature (**Figure 16**). The reflectance was recorded as described above and a temperature controller connected to a hotplate was used to determine the temperature. Since the fading of color in synthetic hackmanites is induced both with heat and light, a second measurement had to be done without heating to determine the fading rate induced by the light bulb used for illumination. Once this was done, the effect of light-stimulation could be removed from the TT measurement to reveal the effects of heating alone. The energy required for color removal was evaluated from the TT with the initial rise method presented earlier in Chapter 4.2.2.
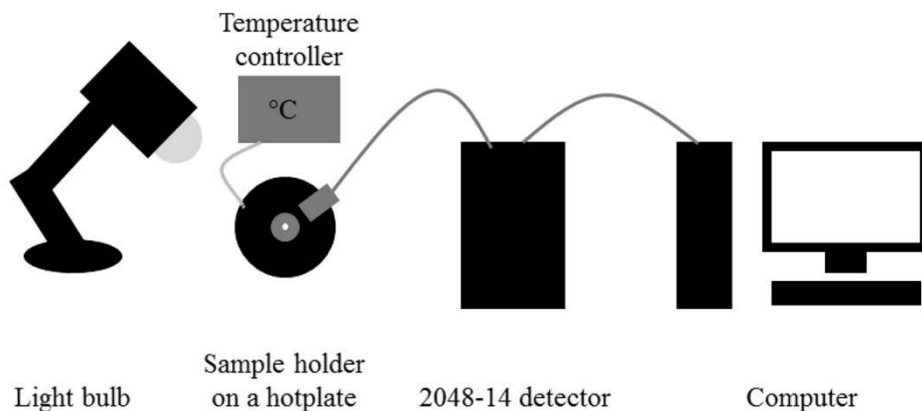
Figure 16 Schematic overview of the thermotenebrescence measurement setup including light bulb, temperature controller, sample holder and hotplate, 2048-14 detector, and the computer to record the data from the measurement.

The color of the samples was also determined from photographs taken of the samples. In this case ImageJ program [96] was used to determine the color intensity in the picture. The program calculates the RGB value of the selected area and the different RGB values of different samples can be used to compare the color intensity of the samples.

4.2.4. Computational methods

In addition to experimental methods, computational calculations were also used to get more detailed results from the hackmanite material. The calculations were carried out using a 2x2x2 supercell of the primitive sodalite unit cell that had a chloride vacancy V_{Cl} in the center. For the geometry optimizations the reciprocal space was sampled using Γ point as a single k-point. The doping concentration of 6.25% for S_2^{2-} ion was chosen in comparison to chloride concentration resulting in one chloride being replaced with S_2^{2-} in the supercell.

Computational work aimed in determining the most probable doping site for cations replacing Na in the system. Four different sites (a–d) were considered being either in the proximity of V_{Cl} and/or S_2^{2-} or neither (**Table 8**).

Table 8 Na sites a–d used in computational measurements and their location in relation to V_{Cl} and S_2^{2-}.

Site	Close to V_{Cl}	Close to S_2^{2-}
a	no	yes
b	yes	yes
c	yes	no
d	no	no

After this, the computational method was used to study the mechanism of photochromism in synthetic hackmanites. For the calculations several doping concentrations for cations in Na site were used between 0 and 4.8%. The calculations were used to study the effects the doping had on the gaps between conduction band, highest occupied orbital and lowest unoccupied orbital.

All computational calculations were carried out using Density Functional Theory (DFT) framework [101] and the global hybrid functional PBE0 in periodic boundary condition (PBC) with the *ab initio* CRYSTAL14 code. A fixed value of 10^{-7} Ha per unit cell was used as the convergence criterion for the self-consistent field (SCF) cycle. The localized (Gaussian) basis sets together with solving self-consistently the Hartree-Fock [102] and Kohn-Sham [103] equations allowed the efficient use of hybrid functionals.

For the Na, Si, Cl, Al, O, Li and K atoms the all-electron double-zeta basis set was used with the polarization functions of 85–11G(d), 88–31G(d), 66–31G(d), 86–21G(d), 66–31G(d), 5–11G(d), and 865–11G(d), respectively. For the S atom the triple-zeta basis set 86–311G(2d) was used and for the Rb atom the Hay-Watt small core pseudopotential was used with the 31G(d) basis. Lastly for the electron trapped in V_{Cl}, a basis with the 11G(d) structure was optimized for each system.

In addition to this, density of states (DOS) calculations were conducted using a 4x4x4 k-points mesh. The DOS calculations show the total density of states as well as the DOS projected on S_2^{2-} and V_{Cl} orbitals separately.

5. Results and discussion

5.1. Different compositions of synthetic hackmanites

The solid state synthesis protocol was used to prepare different hackmanite materials. The first step in hackmanite synthesis optimization was to find the proper S/Cl ratio [I]. The results indicated that both Cl and S are needed to produce luminescence and photochromism in hackmanite materials. From the samples that contained both Cl and S, luminescence and reflectance spectra were measured (**Figure 17**). The results indicate that the S/Cl ratios of 0.06 and 0.13 have the best results in both aspects [I]. Since the increasing amount of S in the material results in a redshift in the luminescence color the S/Cl ratio of 0.06 was chosen as the best one and this was then used in most materials. The superiority of the 0.06 material was confirmed with repeating the synthesis a couple of times. The material turned always out better than the other materials. However, minor differences in luminescence and photochromic properties were found between the different samples. Thus, the same sample with S/Cl ratio of 0.06 was used as a reference throughout the thesis.
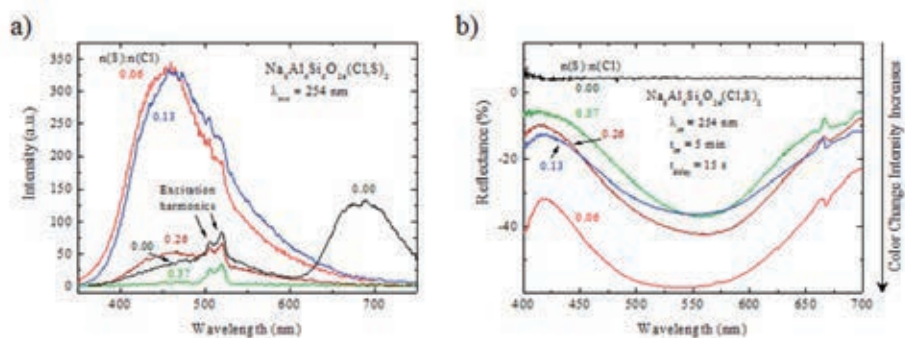
Figure 17 Luminescence (a) and photochromism (b) in synthetic hackmanite samples prepared with different S/Cl ratios (**Table 4**). [I]

In the next phase of the materials preparation Na was partly replaced in the synthesis with other alkali metals. The results showed that partly replacing Na with a lighter element, Li, improved the PL and PeL properties of synthetic hackmanites [III] whereas the substitution with heavier elements, K and Rb, improved the photochromism of the materials [IV]. The same results were also obtained from computational work [IV]. Replacing Na with Li increases the energy gap between S_2^{2-} and V_{Cl} (**Figure 18**). The increase in gap energy prevents the efficient trapping of electrons in V_{Cl} required in photochromism. Since PeL and photochromism are somewhat competing phenomena in synthetic hackmanites the decrease in photochromism allows more energy to be used in PeL thus enhancing this phenomenon. [IV]
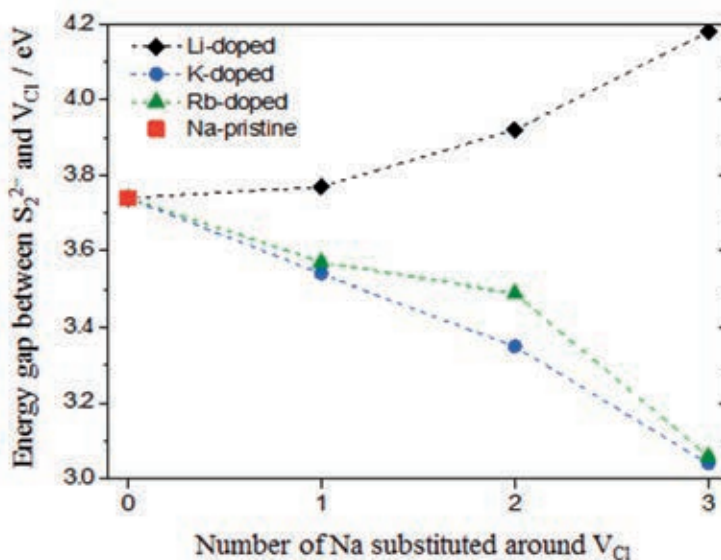
Figure 18 Computed results on the effect of Na substitution around V_{Cl} in the energy gap between S_2^{2-} and V_{Cl} [IV].

Computational results shown in **Figure 18** support the experimental findings that K and Rb substitution results in materials with stronger photochromism. This happens when the S_2^{2-} – V_{Cl} gap becomes smaller and thus the electrons are trapped more easily to form color centers. The photochromism mechanism becomes then dominant over the PeL mechanism. [IV]

To enhance the PL intensity and lengthen the duration of PeL, Li-hackmanite was then doped with different elements to find the optimal composition for luminescence in hackmanites. The luminescence properties were then enhanced even further by introducing boric acid in the synthesis as a flux to help the arrangement of ions as well as to increase crystal growth during synthesis. [I–III]

To study the possibility of hackmanite materials acting as host materials for up-conversion luminescence, the basic hackmanite with S/Cl ratio of 0.06 was doped with different amounts of ytterbium and erbium, which have good records in producing up-conversion luminescence in different host materials [63]. [V]

Since the results indicated that luminescence properties and photochromism in synthetic hackmanites can be enhanced with different compositions, the research focused on preparing synthetic hackmanites for optimal luminescence properties and also on other materials that have strong photochromic properties. In the last step the material composition was optimized to yield a material with all optical properties possible in one material. This multifunctional material could then be used in optical multiplexing [V].

5.2. Purity in materials

The purity of prepared materials was first studied with XRD. The results showed that in most materials some alkali metal chloride was present as an impurity either as an unreacted starting material or resulting from the decomposition of formed hackmanite. This impurity was successfully removed from the sample when it was washed with quartz distilled water. After the washing only a small amount of $RbAlSiO_4$ was present as an impurity in Rb-hackmanites [IV]. This impurity was concluded to be minor and not affecting the optical properties of Rb-hackmanite.

From the XRD results obtained, Rietveld analysis was carried out to determine the unit cell volume of prepared materials. The first results showed an increase in unit cell volume with increasing sulfur content with the exception of the sample with S/Cl ratio of 0.06 [I]. The increase was expected since the ionic radii 1.84 Å for S^{2-} is larger for that of 1.81 Å for Cl^- in 4-coordination [104]. The composition with S/Cl ratio of 0.06 might be somehow optimal for the material since it differs from other samples in the series in optical properties as well, as can be seen later.

Rietveld analysis was also used to calculate interatomic distances in hackmanite material. In the case of ytterbium and erbium doped materials, the information from Rietveld analysis was used to evaluate whether the dopants have entered the host lattice. With small dopant concentrations the unit cell parameter *a* decreases clearly. This indicates that the dopants have entered the material causing changes in the unit cell size. With higher concentrations, the

(Yb,Er)$_2$O$_3$ impurity phase forms decreasing the amount of dopant concentration in the hackmanite material. This is supported by the fact that with higher doping concentrations, the unit cell parameter *a* is more close to that of non-doped material. [V]

After XRD, the chemical composition was studied with XRF. The source of impurities in the final product was discovered to be in the zeolite starting material. The XRF results for elements present in zeolite starting material in a quantity of at least 0.1‰ are listed in **Table 9**. The impurity elements found in zeolite proved to be really important for the luminescence properties of synthetic hackmanites (see **5.3**). [I]

Table 9 XRF results of zeolite starting material [I].

Element	Content (%)	Element	Content (%)
Si	48.6	Mn	0.01
Al	34.3	Fe	0.04
Na	16.2	Ti	0.03
Cl	0.66	Ca	0.03
K	0.10	S	0.01

The XRF measurement was also used to study the S/Cl ratio of the prepared materials. The results confirmed that the S/Cl ratio, after subtracting the amount of Cl resulting from the NaCl impurity phase, was the same in the final product as calculated from the amounts of starting materials used [I]. This confirmed that the synthesis was successful and Cl and S have entered the hackmanite structure. In a similar manner the Er/Yb ratio of ytterbium and erbium doped materials was studied (**Table 10**) [V]. Again the results show a close relation between the calculated and measured ratios indicating successful doping.

**Table 10** Calculated and measured Er/Yb ratios for synthetic hackmanite materials. [V]

Sample	Er/Yb cal.	Er/Yb meas.	Sample	Er/Yb cal.	Er/Yb meas.
Yb 3 mol-% Er 1 mol-%	0.32	0.32	Yb 9 mol-% Er 3 mol-%	0.32	0.30
Yb 6 mol-% Er 2 mol-%	0.32	0.36	Yb 20 mol-% Er 6 mol-%	0.29	0.28
Yb 6 mol-% Er 2 mol-% (Cl)	0.32	0.30	Yb 20 mol-% Er 6 mol-% (Cl)	0.29	0.31

After getting the overall idea of the impurities present in hackmanite materials, a more detailed analysis was carried out using ICP-MS. The material studied was a non-doped material with a S/Cl ratio of 0.06. The measurement focused on elements known to act as luminescence centers. The measurement found 4 possible luminescence centers, titanium (content 74 ± 50 ppm), iron (content 136 ± 4 ppm), manganese (content 2 ± 0.4 ppm), and chromium (content 11 ± 1 ppm). Their effects on hackmanite luminescence are discussed in chapter 5.3. [II]

TEM imaging was used to study the materials' stability in aqueous media. The synthesized Li-hackmanite was suspended in water solution for several weeks. After this both the bulk material and suspended material were studied using TEM. The results show that both samples contain large particles that are several micrometers in size and also smaller particles that are about 200 nm in size. The notable difference between these two samples was that with the sample kept in water, the smaller particles had a more regular size. [III]

XPS measurements were carried out to study the oxidation state of sulfur and titanium present in hackmanite materials. The method was also used to study the changes in oxidation state when the material was exposed to UV radiation.

[II–IV] With titanium, there are only two oxidation states present, Ti^{4+} and Ti^{3+}. The Ti^{4+} originating from TiO_2 starting material is the most common state. The reduction of hackmanite samples reduces a part of the titanium to Ti^{3+} that can be seen in the XPS spectra of the final product [II]. With sulfur there is a larger variety of different oxidation states present (**Figure 19**) [IV]. Oxidation states of S^{6+}, S^{4+}, and S^{2-} or S^- are present in the XPS spectrum of white Rb-hackmanite material. Once the material is exposed to UV radiation and the color of the material changes due to photochromism (for more details see 5.4) a new oxidation state of S^0 or $S^{-0.5}$ appears in addition to the old ones. This new oxidation state is related to the photochromism mechanism in hackmanites that is described in chapter 5.4.
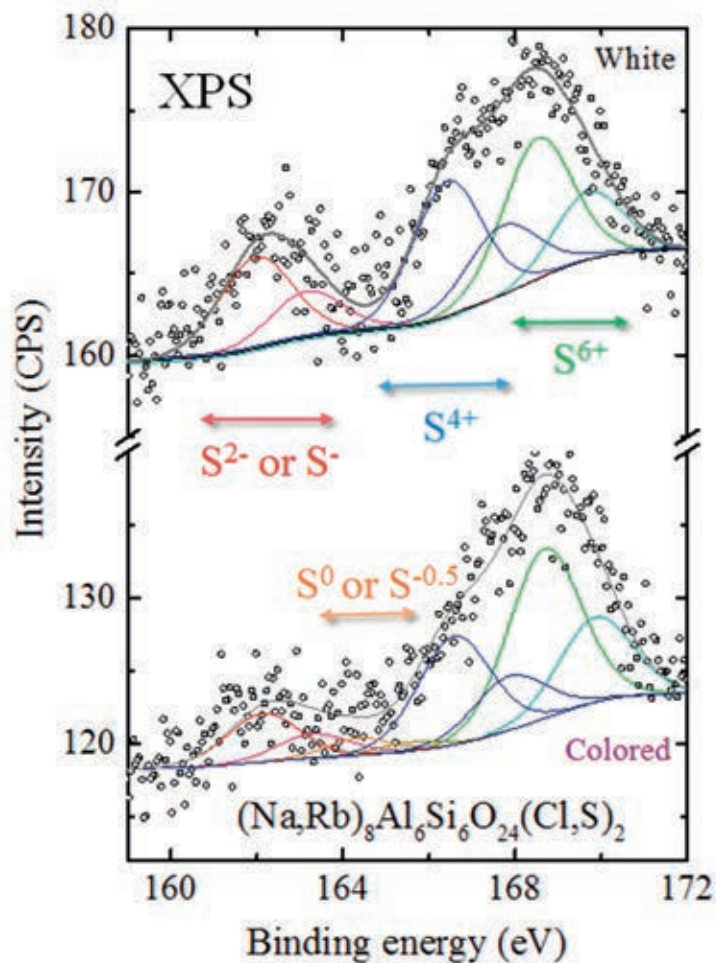
Figure 19 XPS spectrum for Rb-hackmanite in white and coloured form. [IV]

SEM-EDX analyses were conducted to see the distribution of elements (Ti, K and Rb) in selected materials. The titanium measurement was used to prove the even distribution of doped Ti over the whole material. As can be seen from **Figure 20**, the distribution is even and the conclusion can be made that the dopant has entered the hackmanite structure. [II]
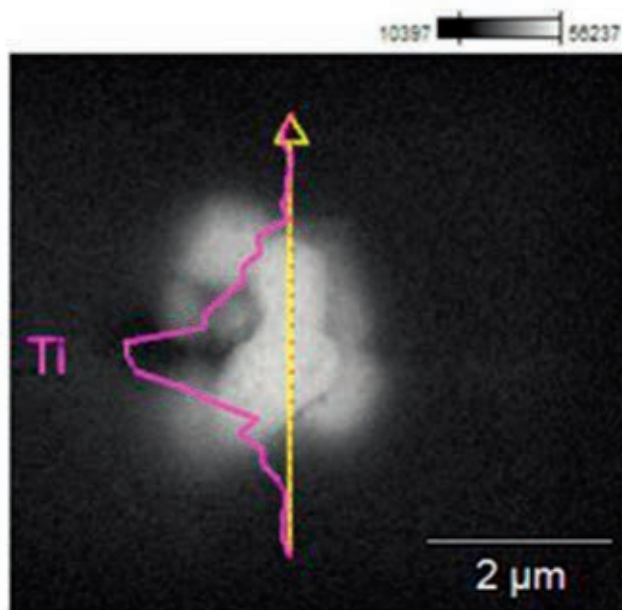
Figure 20 SEM-EDS image of synthetic hackmanite with the S/Cl ratio of 0.06 and 2 mol-% of Ti doping showing the distribution of titanium in the grain. [II]

When studying the SEM-EDX results of K- and Rb-hackmanites the focus was on the success of Na substitution in hackmanite. From both materials 100 particles were chosen at random and their K or Rb composition was determined. According to the synthesis protocol, 25% of Na should be substituted to K or Rb. Despite this, the results showed substitution rates of 14% and 10% for K and Rb, respectively. The results indicated that the doped cations have poor solubility in the Na site, probably due to geometrical difficulties when larger cations (K^+ and Rb^+) try to enter the smaller Na^+ site. [IV]

The changes occurring in hackmanite after UV excitation were studied in more detail using solid state MAS-NMR. Selected samples were measured before and after excitation. The measurements were carried out for ^{23}Na, ^{27}Al and ^{35}Cl. From all spectra measured only ^{23}Na showed a difference between samples before and after excitation. This small but notable shift that could be seen after normalizing the spectrum according to the internal reference of 0.1 molar NaCl in D_2O

(**Figure 21**) turned out to be an important result when confirming the mechanism for PeL (see chapter 5.3.2). [III]
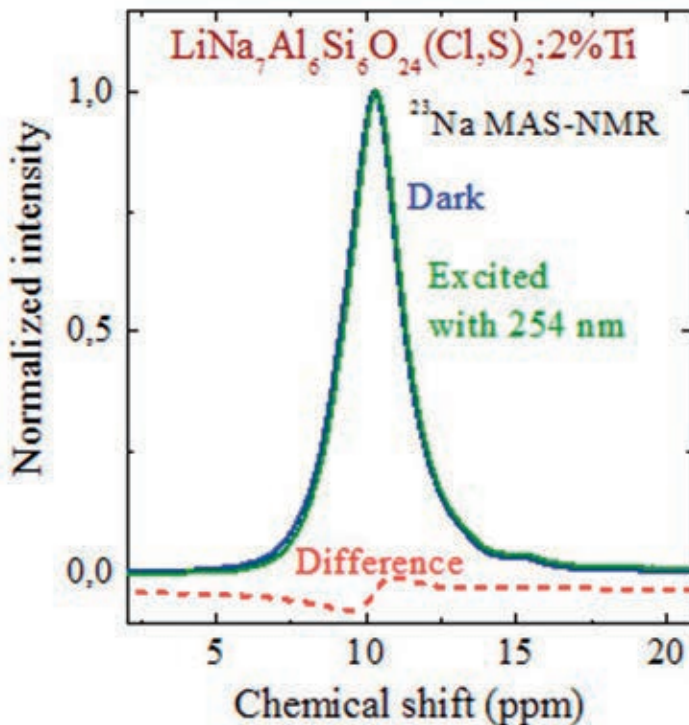
Figure 21 Solid state NMR results of Ti doped Li-hackmanite measured before and after 30 min excitation with 254 nm. [III]

Even if the ^{35}Cl MAS-NMR results didn't show any differences for samples before and after excitation the results could still be used to estimate the amount of F centers present in the materials. The signals present in ^{35}Cl MAS-NMR spectra at *ca.* −132, −52 and +2 ppm are attributed to the regular, vacancy free form of sodalite, to the NaCl impurity present in the material, and to the chloride ions close to a high number of F centers, respectively. [I] The signal close to −130 ppm was also used to estimate the concentration of F centers in the whole material. It has been shown before [105] that the signal moves to lower ppm values with decreasing concentration of F centers. The obtained value of *ca.* −130 ppm for hackmanite, K-hackmanite and Li-hackmanite indicates that the

actual concentration of F centers is significantly lower that the nominal concentration of 5%. [IV]

The results obtained from EPR measurements were also used to study the structure and especially the changes taking place in the structure after the excitation of the sample. Selected samples were measured with EPR before and after excitation at 355 nm or 254 nm. The data from the non-irradiated sample shows signals attributed to Mn^{2+} which is present as an impurity in the material as confirmed earlier by ICP-MS and XRF. When exciting the material with 355 nm the selected hackmanite with S/Cl ratio of 0.06 exhibits PeL but not photochromism. The EPR results of this material show a similar structure to the non-irradiated sample. The only difference occurs at 3510 G. This change is thus the result of the unpaired electrons resulting from the PeL mechanism. In the same manner, the sample was excited at 254 nm. With this excitation the material exhibits both PeL and photochromism. To be able to study the effects of photochromism alone the material was kept in the dark for one week after the excitation. After this time there is no longer PeL since it discharges on its own after the excitation ends. Photochromism on the other hand stays in the material when kept in the dark. After one week the EPR was measured and the results showed that the signal attributed to PeL mechanism was no longer present. Instead a new feature at 3517 G was present which could then be taken to be resulting from unpaired electrons from photochromism (**Figure 22**). [II]
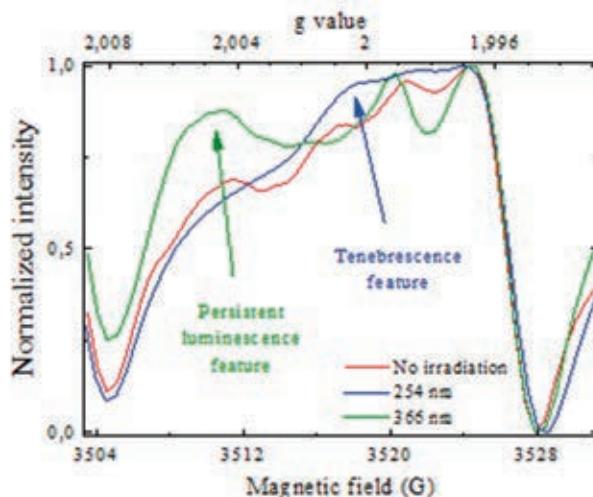
Figure 22 EPR spectra measured from synthetic hackmanite before and after excitation with 254 and 365 nm. [II]

EPR measurements were also carried out for Ti doped Li-hackmanite. In this material the presence of Ti^{3+} is clearly observed. When excited, the signals for Ti^{3+} decrease which is a result of Ti^{3+} being oxidized to Ti^{4+}, which does not have any unpaired electrons and can thus not be seen in EPR spectra. This oxidation is closely related to PeL mechanism which is discussed in more detail in chapter 5.3.2. [III]

Lastly the, FTIR measurements of a hackmanite sample with S/Cl ratio of 0.06 before and after excitation confirm the different structural changes taking place during luminescence phenomena and photochromism. While the IR spectra for non-irradiated and 365 nm irradiated samples are identical, the spectrum for 254 nm irradiated sample shows a change at the signal at *ca*. 1000 cm^{-1} that can be assigned for asymmetric T–O–T (T = Si, Al) bending [106]. This shows that luminescence induces changes in the structure that is not IR active and photochromism induces changes observable via IR. [II] The different properties and their mechanism are discussed in chapters 5.3 and 5.4**.**

5.3. Luminescence properties

Like natural hackmanites, synthetic hackmanites show photoluminescence when excited with UV. The synthetic hackmanites also exhibited strong persistent luminescence, unlike their natural counterparts that usually do not show PeL and if they do, it only lasts for a couple of minutes. The first observations showed that synthetic hackmanites can have different luminescence properties depending on the composition and the excitation source. This led us to study the different luminescence properties and the mechanisms behind them.

5.3.1. Photoluminescence

This work's first observations of PL in synthetic hackmanites were made after the first synthetic hackmanite series, the different S/Cl ratios, was made. This series showed clearly the range of different luminescence properties that can be obtained from synthetic hackmanite (**Figure 23**). The different S/Cl ratios all show PL with different colors and the color also depends on the excitation wavelength. When sulfur is present in the sample, the emission maximum shifts to a higher wavelength.
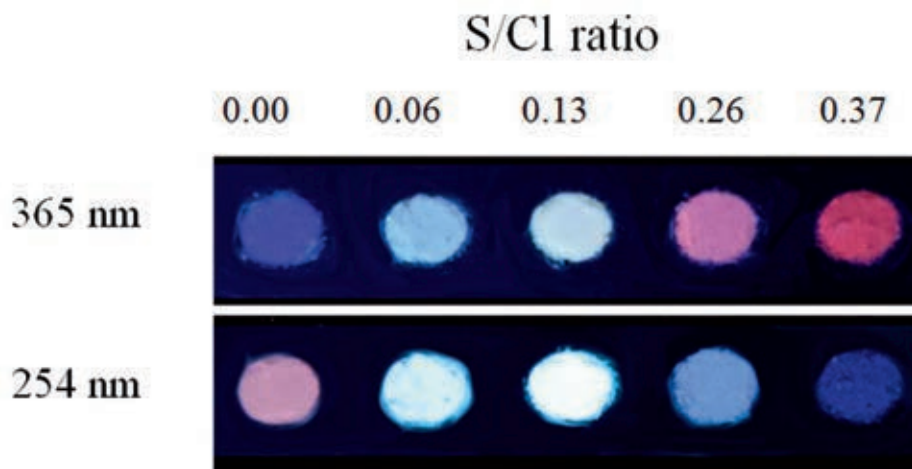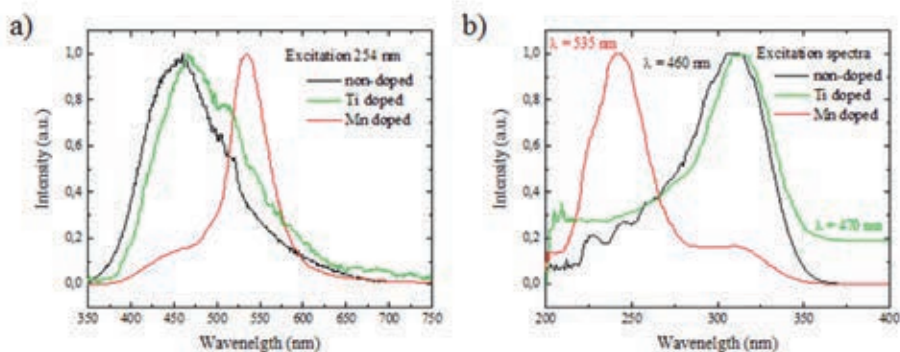

Figure 23 Luminescence in synthetic hackmanites prepares with different S/Cl ratios (**Table 4**) and excited with 365 and 254 nm. [I]

Since the hackmanite luminescence is strongly dependent on the excitation wavelength, the luminescence excitation spectrum was measured for the samples with different S/Cl ratios. The emission wavelength of about 460 nm was chosen to be measured since it is the center of the main emission peak. For all samples the excitation spectrum was similar and it had the maximum at 310 nm. Below 310 nm the excitation spectrum drops fast meaning that higher energies will not excite the PL efficiently.

To get a better understanding of the PL of synthetic hackmanite, the luminescence center needed to be determined. Based on XRF and ICP-MS measurements discussed above, the luminescence center could be determined to be one of the following: titanium, chromium, manganese or iron. Since the main emission peak of hackmanite has its maximum at about 460 nm, we could discard chromium and iron, since they are known to have mainly red luminescence and thus can not contribute to the 460 nm emission [107]. After this, the effects of titanium and manganese on synthetic hackmanite PL were tested by preparing hackmanite samples with 2 mol-% doping of Ti or Mn.

The prepared Ti and Mn doped samples were compared to a non-doped sample to better understand the effects of doping in hackmanite luminescence. In **Figure 24** we can see that the titanium doping has a minimal effect on both luminescence emission and excitation spectra compared to the non-doped sample. Manganese doping on the other hand changes the shape and the position of both emission and excitation spectrum. This highly suggests that manganese is not responsible for hackmanite luminescence.

Figure 24 Normalized spectra of hackmanite a) emission and b) excitation in non-doped as well as Ti and Mn doped hackmanites. Adapted from [II].

The shape of the PL spectrum of synthetic hackmanite suggests that there might be more than one luminescence centers responsible for the PL. Since O_2^- has been known to show blue luminescence in minerals, the possibility of its contribution was tested. Synchrotron measurements carried out at 20 K showed the typical vibrational bands with ca. 1000 cm^{-1} intervals located at 400 nm. This suggests that both O_2^- and titanium are responsible for the PL in synthetic hackmanites. The fading time for O_2^- luminescence is generally a lot faster than that of titanium. Therefore, the emission decay times recorded at different emission wavelengths suggest that the O_2^- luminescence dominates the blue side of the emission peak while titanium dominates the red side (**Figure 25**). [II]
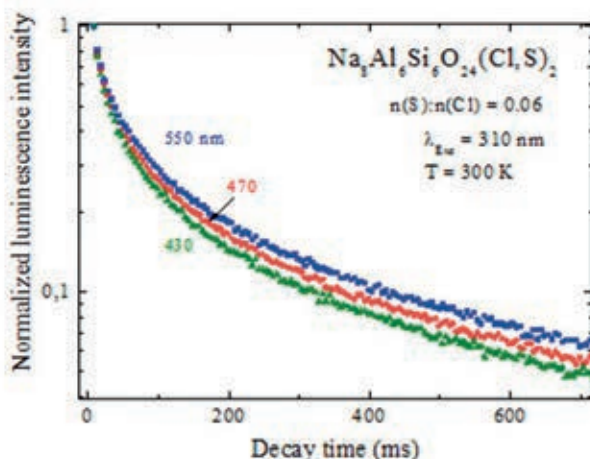
Figure 25 Emission decay curves for synthetic hackmanite with S/Cl ratrio of 0.06. The curves have been recorded at different emission wavelengths. [II]

The location of the doped titanium was then assumed to be in the Al^{3+} site in the synthetic hackmanite. The ionic radius of four-coordinated Ti^{4+} (0.42 Å) is closest to that of four-coordinated Al^{3+} (0.39 Å) [104]. The other possible sites in hackmanite are four-coordinated Na^{+} (0.99 Å) and four-coordinated Si^{4+} (0.26 Å). From these, the titanium could possibly also occupy the Si^{4+} site because of the match in the valence. XPS results then showed that in synthetic hackmanite, both Ti^{3+} and Ti^{4+} are present. The titanium in the starting material TiO_2 is only in the form of Ti^{4+} but during the reduction part of the hackmanite synthesis, a part of Ti^{4+} reduces to Ti^{3+}. [II]

The total luminescence process for synthetic hackmanite PL was then concluded to happen in a close pair of titanium and oxygen vacancy (Ti^{3+}–V_O• pair) when electron excites from Ti^{3+} to V_O• and a charge transfer then happens from V_O• to Ti^{4+}. [II]

Once the mechanism for PL was confirmed, efforts could be made to make the luminescence stronger. When looking into the mechanism of photochromism that will be discussed in chapter 5.4 it can be seen that replacing sodium partly with lithium will allow the PL to be stronger. This is because the presence of lithium

raises the energy needed for photochromism and thus more energy is left for the luminescence phenomena. This was supported by the preparation of Li-hackmanites. The prepared Li-hackmanite with an alkali metal composition of LiNa$_7$ (compared to Na$_8$ of original, synthetic hackmanite) showed even stronger PL than the hackmanites synthesized before. [III]
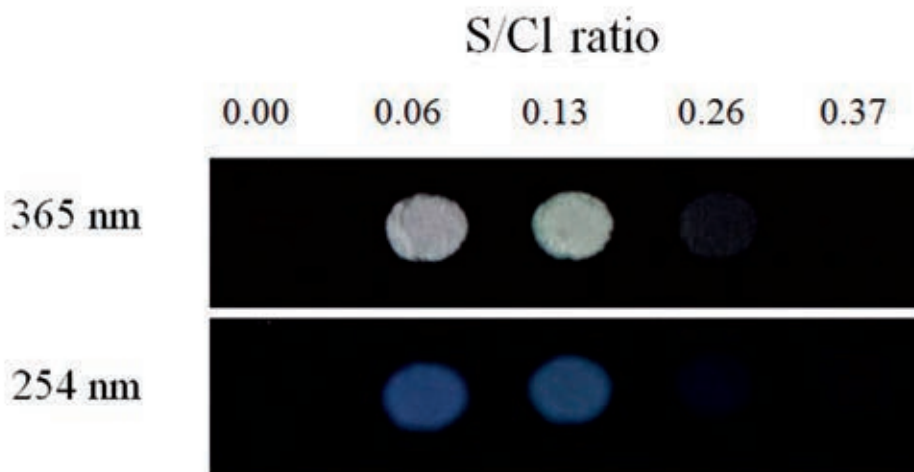
The synthetic hackmanite shows luminescence in different colors ranging from blue to red. The excitation wavelength strongly affects the color and intensity of the luminescence. This study focused mostly on the blue/white PL, since this is not studied before as widely as the red/orange PL of natural hackmanites. The strongest luminescence in synthetic hackmanites can be obtained with 310 nm excitation. Maybe the most interesting property of hackmanite luminescence is that it can produce white luminescence with a broad emission. For example the PL of LiNa$_7$ hackmanite doped with 2 mol-% titanium is white according to the CIE color coordinates assigned to white by Fortner and Meyer [108] (**Figure 26**) [III].
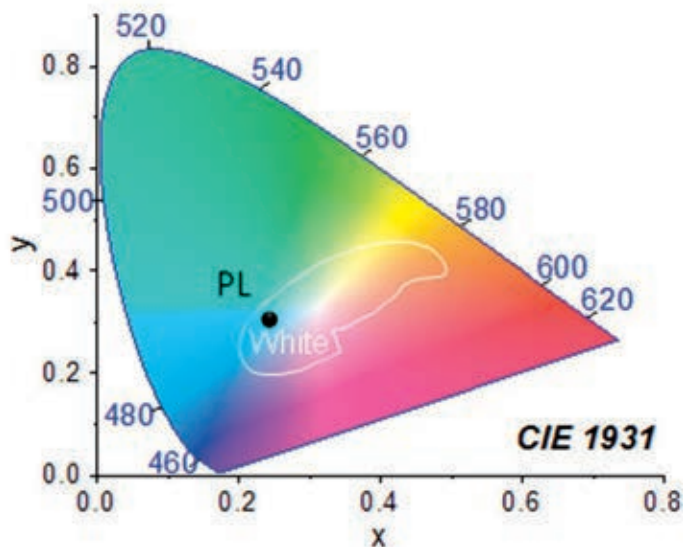
**Figure 26** CIE color coordinates for synthetic Li-hackmanite PL. [III]

5.3.2. Persistent luminescence

Persistent luminescence in synthetic hackmanites was first reported by us in 2015 [I]. The phenomenon opened a wide new research area in synthetic hackmanites. Not all synthetic hackmanites show PeL and the color and intensity of persistent luminescence varies in the samples widely (**Figure 27**). The first observation was that the sample that did not contain sulfur did not have any PeL observable either in photographs or with a spectrometer [I]. This suggests that sulfur might play an important role in the mechanism of persistent luminescence in synthetic hackmanites.

Figure 27 Persistent luminescence in synthetic hackmanites prepares with different S/Cl ratios (**Table 4**) and excited with 365 and 254 nm. [I]

The mechanism of PeL was then studied in more detail. Since titanium was determined to be responsible for the photoluminescence in synthetic hackmanites it was also studied in the case of persistent luminescence. The comparison was made between non-doped and Ti-doped hackmanites with the S/Cl ratio of 0.06 (**Figure 28**). The shape of the emission spectra is similar in both samples. However, the intensity and duration of PeL in the titanium doped sample is superior to the non-doped sample. [II]
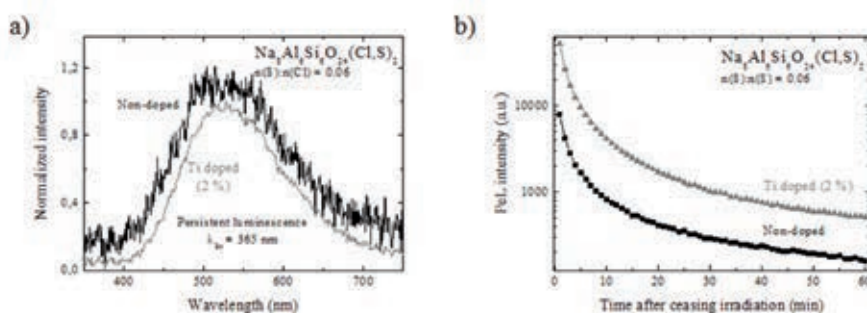

Figure 28 PeL a) emission and b) decay in non-doped and Ti-doped synthetic hackmanites. [II]

The comparison of PL and PeL spectra of synthetic hackmanites shows that the shoulder clearly visible in the PL spectra on the higher wavelengths

(**Figure 24** a) is not present in the PeL spectrum. This suggests that the PeL originates from just one luminescence center, contrary to PL.

During the investigation of the luminescence centers with synchrotron excitation a blue-shift was noticed in the luminescence spectrum when compared with the data obtained with the regular laboratory setup. The shift is due to the different delay time in the synchrotron measurements compared to the conventional luminescence measurements. When the matter was studied in more detail it was clear that the emission maximum shifts to higher wavelengths with the increase in delay time. When the time increases enough so that there is no PL left, the position of the PeL emission spectrum becomes fixed and no longer moves with increasing delay time (**Figure 29**). This finally confirms that the mechanism of PeL involves only one luminescence center whereas PL has two different centers.
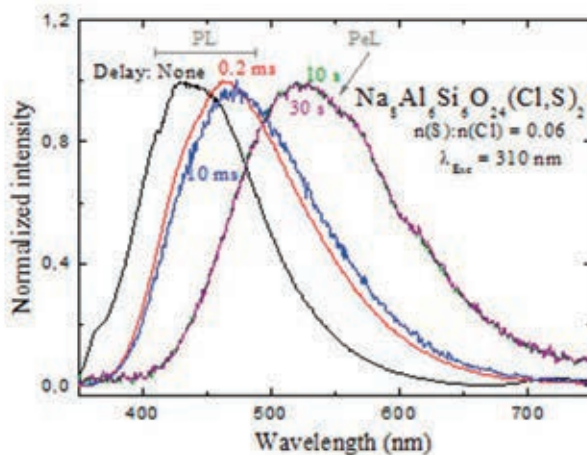
Figure 29 Hackmanite emission with different delay times with 310 nm excitation. [II]

The thermoluminescence measurements carried out for non-doped synthetic hackmanite with S/Cl ratio of 0.06 after excitation with 254 nm showed two different peaks in the TL glow curves. This indicates that there are two traps with different energies within the hackmanite material. By preheating the material to 250 °C the second trap locating at *ca*. 300 °C was revealed. After this the energies

of both traps were calculated with the initial rise method [100]. The energies for the shallower and deeper traps are 0.5 and 1.2 eV, respectively. The deeper trap is not observed in the TL curve when the excitation is made with 365 nm (**Figure 30**). [II]
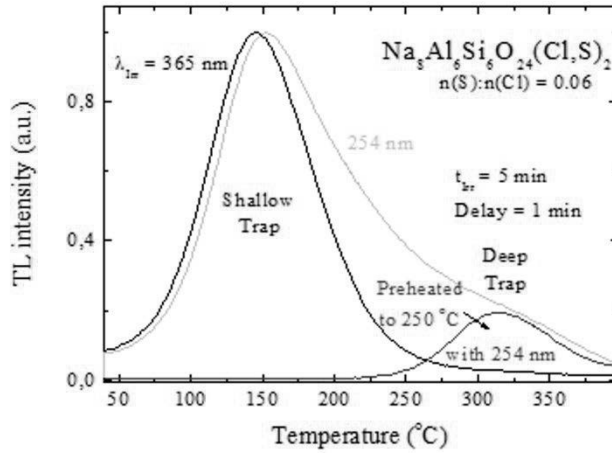
Figure 30 Thermoluminescence glow curves for synthetic hackmanite with S/Cl ratio of 0.06. Sample was excited with 254 and 365 nm. [II]

Based on the results presented above, the mechanism for PeL in synthetic hackmanites was concluded to take place in a Ti^{3+}-V_O pair. The energies of 3.4 eV and more are absorbed by the pair and electrons are transferred to the conduction band. From there, the electrons are trapped in the oxygen vacancies that lie 0.5 and 1.2 eV below the conduction band. When electrons are released from the traps by thermal energy, they migrate to the excited levels of Ti^{3+} from where they relax emitting a photon at 2.4 eV. This results in the PeL visible at 515 nm (**Figure 31**).
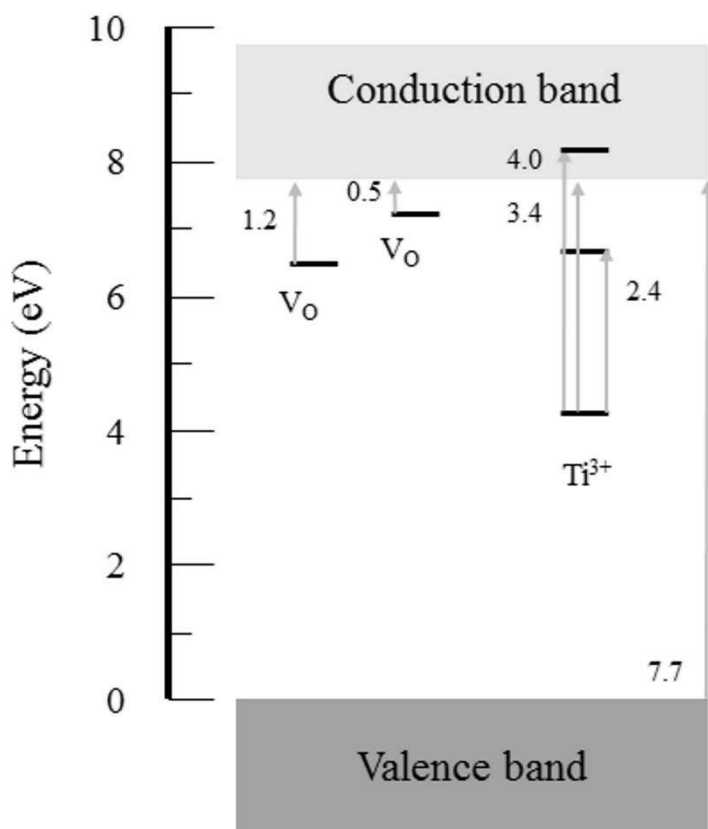
Figure 31 A schematic of the energies involved in the persistent luminescence mechanism of synthetic hackmanites. Modified from [II].

The efficiency of PeL can best be measured by the duration of the luminescence. First, the duration was measured with a luminescence spectrometer after 30 min of excitation with a 254 nm UV lamp. The measurement was carried out for 100 h measuring the spectrum every 30 min. At the end of the measurement the spectrometer was still able to detect the luminescence from the Ti-doped Li-hackmanite material (**Figure 32 a**). Another good way to measure the length of the PeL is to record its luminance and determine the time the intensity stays above the limit of 0.3 mcd m^{-2} [98] set by the industry. The same measurement was carried out for commercial phosphors in use today to compare the new Li-hackmanite to other materials (**Figure 32 b**). The measurement shows

that while commercial $SrAl_2O_4$ and $Sr_2MgSi_2O_7$ doped with Eu and Dy are superior to the new material, synthetic hackmanite can match the length of commercial $CaAl_2O_4$ doped with Eu and Nd and it exceeds the length of Y_2O_2S doped with Eu, Ti and Mg by hours. The advantage of the present Li-hackmanite is that it does not contain expensive lanthanides unlike all of the commercial phosphors. [III]
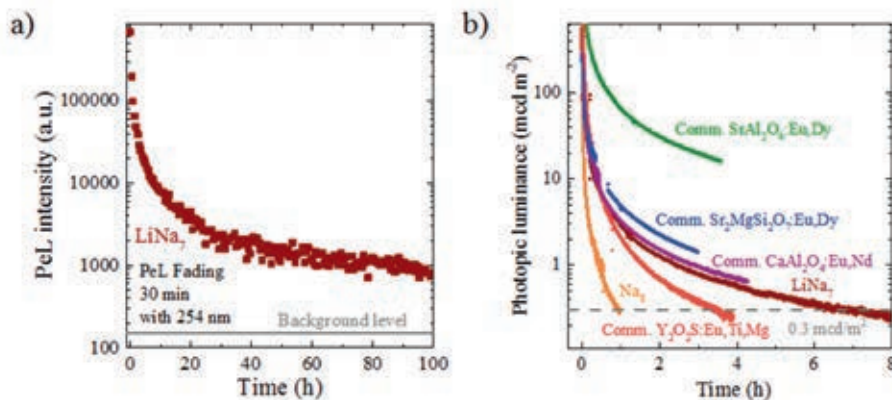
Figure 32 a) PeL of Ti-doped Li-hackmanite measured with a luminescence spectrometer after 30 min excitation with 254 nm. b) Comparison of luminance in Ti-doped Li-hackmanite and comercial phosphors after 30 min excitation. [III]

The color of the PeL emission depends on the composition of the material similarly as in the case of PL. With suitable composition, for example Ti-doped Li-hackmanite, the color of PeL falls to the white category in the CIE coordinates [108]. The color temperature of the PeL is 7556 K which corresponds to cool white. [III]

5.3.3. Up-conversion luminescence

To study if hackmanites could act as host materials for up-conversion luminescence, synthetic hackmanites with ytterbium and erbium doping were prepared. The Yb/Er ratio was chosen based on previous results in different host materials indicating that the ratio produces efficient up-conversion luminescence [109]. The samples were prepared using both lanthanide oxides and lanthanide

chlorides as starting materials. This way it was possible to study in which form the lanthanides can be best introduced to the hackmanite host lattice.

All synthesized samples show up-conversion luminescence but the intensity in the samples prepared from oxides is 5 times stronger than the intensity in the chloride samples (**Figure 33**). In the oxide samples the up-conversion luminescence resulting from the $^4F_{9/2} \rightarrow {}^4I_{15/2}$ transition (650-700 nm) increases with the increasing lanthanide concentration. The increase in the luminescence intensity is natural, since the samples then have more luminescence centers. This is why the luminescence intensity was also compared to the molar amount of ytterbium in the sample. In this comparison the sample with the lanthanide composition of 3 mol-% Yb and 1 mol-% Er stands out. [V]
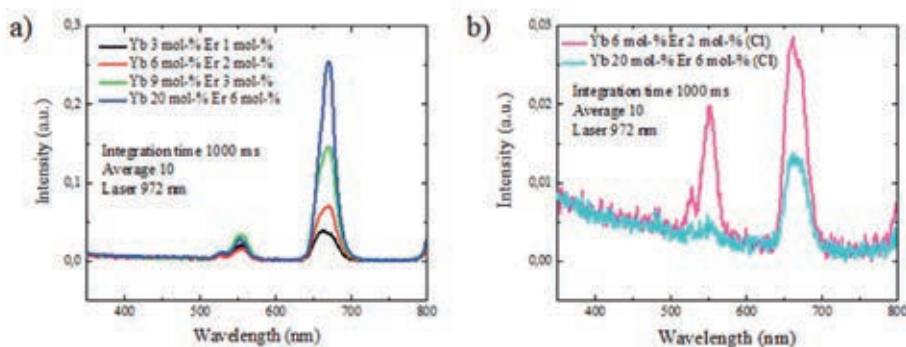
Figure 33 Up-conversion luminescence in synthetic hackmanites under 972 nm excitation. Samples are prepared using a) lanthanide oxides and b) lanthanide chlorides. [V]

When using lanthanide chlorides the diffraction results show intense reflections originating from non-reacted lanthanide chlorides. This together with the luminescence results suggests that ytterbium and erbium have difficulties entering the host lattice, when chlorides are used as starting materials. Thus, lanthanide oxides should be used when preparing up-conversion materials using synthetic hackmanites as hosts. [V]

The doping of ytterbium and erbium into hackmanite structure did not change the shape of the PL or PeL spectrum of the hackmanite. The PL intensity was

comparable to the non-doped sample and in some cases the up-converting samples had even stronger PL than the non-doped sample. In the case of PeL the incorporation of Yb and Er to the lattice decreased the intensity. Nevertheless, all the lanthanide doped samples show notable PeL emission when excited with 365 nm. The decrease in PeL is probably due to the charge compensation after Na^+ sites are filled with Yb^{3+} or Er^{3+} anions. This results in oxygen vacancies being filled and because they are responsible for storing the energy in PeL, the intensity decreases. [V]

The results show that synthetic hackmanite can be used as a host material for up-conversion luminescence. The property could not be optimized during this work but the current results give a good starting point for further research. This also widens the possibilities of different optical outputs if the hackmanites were to be used in sensors.

5.4. Photochromic properties

The photochromic properties of hackmanite have been known since the discovery of the natural hackmanite. The ability to reversibly change color with UV irradiation made the mineral an interesting topic to study. Now also the synthetic version of hackmanite is studied for its photochromic properties.

Like with luminescence, in this work the study of photochromism started from the comparison of the structural differences to the observed properties. Photochromism was studied for the samples prepared with different S/Cl ratios under 254 and 365 nm excitation. The color did not change under 365 nm but the excitation with 254 nm made most of the samples turn purple (**Figure 34**) [I]. The only sample not turning purple was the sample with no sulfur. This confirmed the assumption that sulfur plays a role in the mechanism of photochromism. Interestingly, the sample with S/Cl ratio of 0.00 actually bleached during the 254 nm excitation which can be seen from both the photo (**Figure 34**) and the measured reflectance spectrum [I].
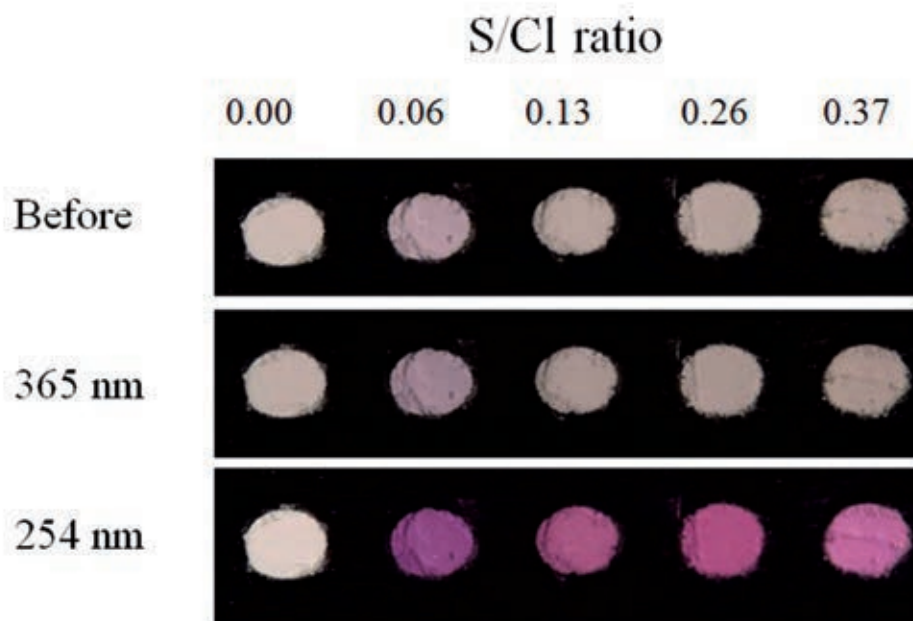
Figure 34 Photochromism in the synthetic hackmanites prepared with different S/Cl ratios (**Table 4**) before the excitation and after they have been excited with 365 or 254 nm. [I]

In addition to photographs and visual observation, another way of measuring the photochromism in the synthetic hackmanites was needed. For this, the measurement of reflectance proved to be the most suitable. The reflectance of the material was measured before and after excitation. When the starting spectrum was deducted from the latter, the intensity of the color change could be seen. The difference curve showed a broad spectrum with a minimum located around 550-560 nm. This corresponds to the purple color also visible with naked eye. [I]

The duration of the photochromism was also studied. The study was made with the sample with S/Cl ratio of 0.06 since it has the strongest color change of the prepared samples. It is known that some optical stimulation is needed to change the color of photochromic materials back to their original state. That is why the sample was illuminated with a light bulb during the experiment. The results and observations show that with naked eye the purplish color can be

observed for about 48 h and even after 60 h the color change can still be observed with reflectance spectrometry. [I]
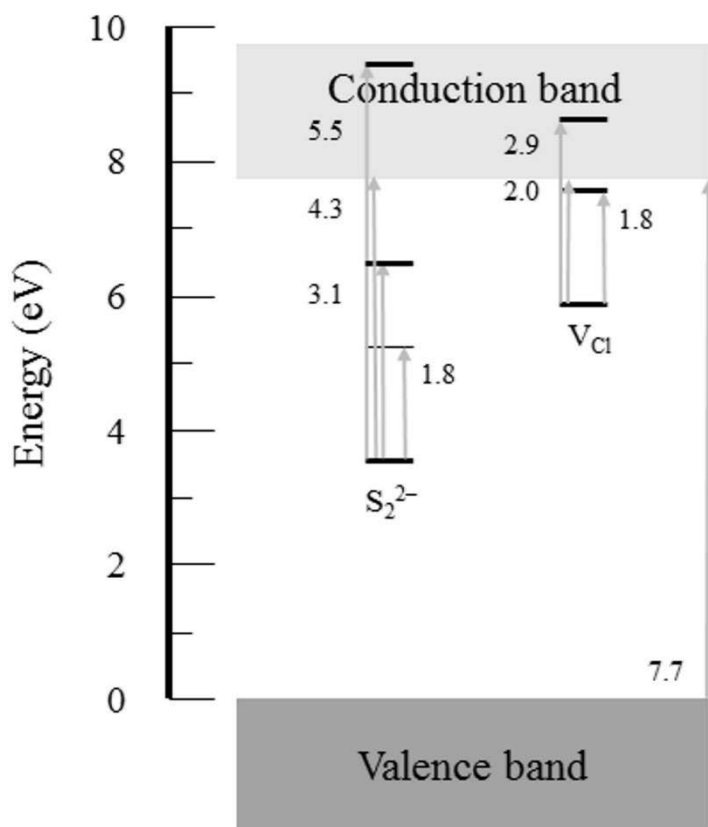
The mechanism of photochromism in the synthetic hackmanite was then studied in more detail. The findings about the importance of sulfur for the photochromism mechanism are also supported by literature [10,12]. The question still remains as to what form the sulfur is in. The sulfur can be present either as S^{2-}, S_2^{2-} or S_2^{-}. Since the mechanism proposed for tenebrescence before [10] involves an electron transferring from the sulfur to a V_{Cl} resulting in a color center and a sulfur radical, effort was made to identify this radical from the colored hackmanite material. The emission spectrum made with 155 nm synchrotron-radiation excitation show a band at 685 nm that could be attributed to S_2^{-} based on the vibration peaks that are present in the spectrum [II] with a 500 cm^{-1} separation. This indicates that the mechanism for photochromism in synthetic hackmanite involves an electron being exited from S_2^{2-} to a V_{Cl} creating a S_2^{-} radical.

Next, the energies involved in photochromism were studied. The first part was to find the energy needed to color the material. For this, synthetic hackmanite was excited with different wavelengths and the reflectance was measured (**Figure 35**) [II]. From these measurements the energy needed to induce the color change in the hackmanite material was found to be 4.3–5.5 eV. Next, the energy needed to remove the color was studied with a similar measurement after first coloring the sample with 254 nm. The energy needed to totally bleach the color is 2.0–2.5 eV (**Figure 35**). [II]
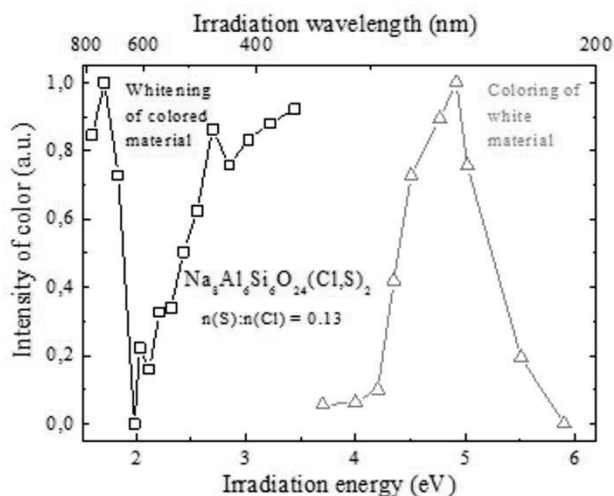
Figure 35 The energies coloring and bleaching the synthetic hackmanite materials. [II]

The last energy needed to complete the mechanism is the absorption of the color center. The material appears purple when it is in the colored state. The reflectance measurement shows the absorption to be between 425 and 700 nm corresponding to 1.8–2.9 eV. In the first part of the photochromism, the S_2^{2-} ion absorbs at 4.3 eV and an electron is lifted to the conduction band. From there, the electron can transfer to V_{Cl} and a color center is formed. The color center can then absorb energies of 1.8–2.9 eV giving the material its purple appearance. From there the electron can get back to the conduction band and transfer back to S_2^{2-} ion gradually fading the color of the material (**Figure 36**). [II]

Figure 36 A schematic of the energies involved in the photochromism mechanism of the synthetic hackmanites. Modified from [II].

For an even better understanding of the photochromism mechanism, some computational measurements were carried out. The first calculations aimed in understanding which Na sites will be replaced with cations when preparing Li-, K- and Rb-hackmanites. The results clearly show that the sites located next to the vacancy (b and c sites, see **Table 8** for details) are the most probable sites (**Table 11**). Only for the K substitution a site further away (d site) is also possible. The preferred substitution around the vacancy is easily explained with the easier adaption of the surroundings for the presence of a different sized cation. [IV]

Table 11 Results from the DFT simulation indicating the energy (E) and distribution (Dist.) of Li, K and Rb cations in different Na sites inside the hackmanite material.

	Site Multiplicity	Li E (eV)	Dist. (%)	K E (eV)	Dist. (%)	Rb E (eV)	Dist. (%)
a	4	0.21	0	0.29	0	0.62	0
b	1	0.00	95	0.31	0	0.47	0
c	3	0.11	5	0.00	16	0.00	100
d	56	0.36	0	0.03	84	0.22	0

Next computations were made on the energies involved in the photochromism mechanism. The first energy involved is the energy between S_2^{2-} and the conduction band. The calculations show that this energy is not affected much by the doping of Li, K or Rb in the hackmanite [IV]. The other energy involved is the energy between the S_2^{2-} and V_{Cl}. The energy of the second gap increases when doped with Li and decreases when doped with K and Rb (**Figure 18**). This is in agreement with the results obtained from the synthetic hackmanites. These results support a direct through space electron transfer instead of a two step excitation and relaxation mechanism for the photochromism (**Figure 37**). [IV]
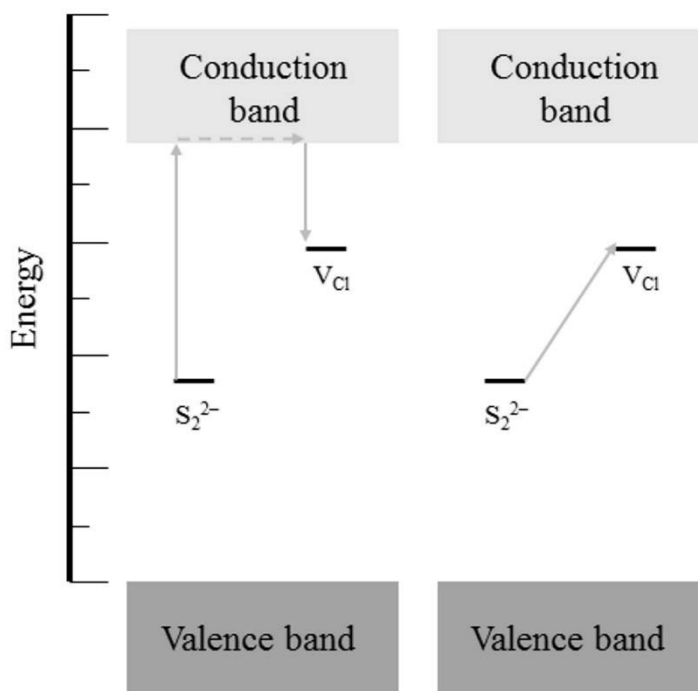
Figure 37 Possible electron transfer routes for color center creation in the hackmanite photochromism. Left: Two step electron transfer. Right: Direct trough space electron transfer. [IV]

The computational results discussed above help understand the mechanism but in addition to that, they also indicate that different hackmanites can be prepared with tunable properties. With the energy gap changing the activation energy for photochromism also changes. This allows the manufacturing of materials in which the photochromism can be induced with different energies. Thus, synthetic hackmanites, K-hackmanites and Rb-hackmanites were prepared and the excitation energies for photochromism was recorded. The results show that photochromism in K- and Rb-hackmanites can be induced with higher wavelengths than in common Na-hackmanites (**Figure 38**). The possibility to tune the excitation energy might prove valuable in possible applications for hackmanites that will be discussed in chapter 5.5. [IV]
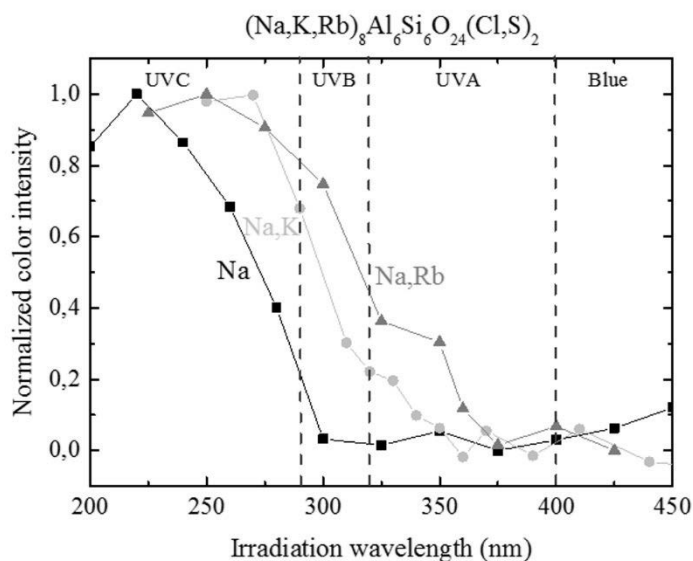
Figure 38 Excitation energies for the photochromism in the different synthetic hackmanites. [IV]

This work's last results about photochromism were obtained with a technique called thermotenebrescence (TT), which was developed during this work. With the new technique it is possible to follow the color bleaching with increasing temperature. Because the measurement is done in lit conditions to be able to measure the reflectance of the sample, the effect of light in the bleaching has to be taken into account. After subtracting this, the TT curves show that bleaching due to light is dominant until 80 °C (K-hackamnite) or 100 °C (Na- and Rb-hackmanite). After this, the thermal bleaching becomes dominant (**Figure 39**). It is also possible to calculate the energy needed to bleach hackmanites from TT curves. When the initial rise method [100] is applied to the obtained TT curves, the energy can be calculated like in the TL case. [IV]
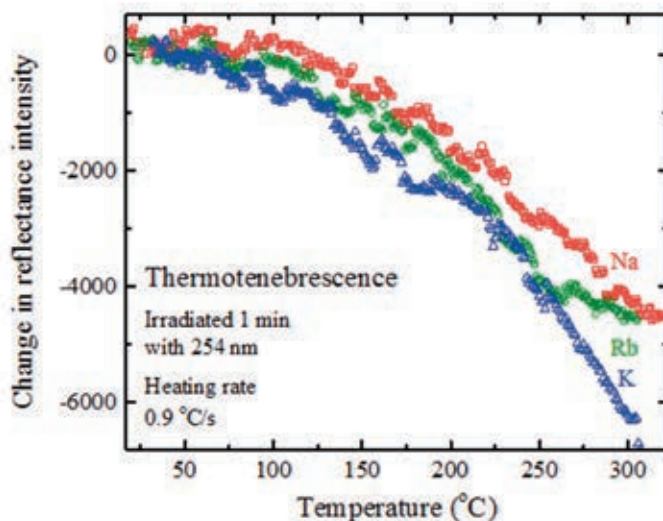
Figure 39 Thermotenebrescence curves for the synthetic Na-, K- and Rb-hackmanites. [IV]

The photochromism property in synthetic hackmanites can be widely tuned with different doping elements. The computational results obtained during the research help to understand the phenomena even more and the deeper insight allows easier preparation of different materials tunable for different applications.

5.5. Possible applications for synthetic hackmanites

The natural mineral hackmanite has some uses mostly in jewelry production, where its photochromic property is valued. Now, the results obtained in this work indicate that the synthetic hackmanites could also have many interesting applications in other different fields.

The white luminescence in the synthetic hackmanites has a wide spectrum and a tunable color. This makes it a promising option for lighting applications. The wide spectrum of the hackmanite luminescence is gentler for human eye compared to the line spectrum obtained from fluorescent lamps in use today. The wide spectrum mimics the spectrum obtained from the sun. The light obtained from the hackmanites is less strong than that of a commercial lighting at the

moment but it is expected to get stronger with more research in the field. The study of quantum yields could give a better understanding of the luminescence, but since it is difficult to measure it from powder samples, it was not measured during the thesis work. Even now the synthetic hackmanite could be used in areas where less brightness is needed, for example in the night time lighting, where the current lights seem too strong. [III]

The results also indicate that hackmanite luminescence can be used in diagnostics. It was proven that hackmanite PL and PeL can differentiate between the expensive spice saffron from its most common counterfeits, turmeric and annatto (**Figure 40**). These promising results suggest that synthetic hackmanites could be used as a label in other kind of diagnostic methods as well. When the fact that the hackmanite luminescence can be exited with sunlight is added to this, it gives the possibility to prepare cheap point-of-care tests using hackmanite that could be used in difficult conditions without any expensive equipment, just using the sun as an excitation source.
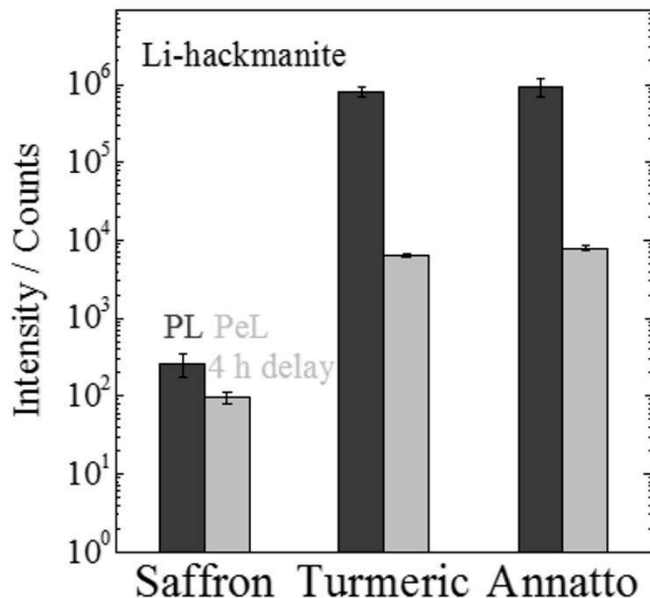
Figure 40 PL and PeL measurements from Saffron, Turmeric and Annatto samples using synthetic Li-hackmanite as a lable [III].

For the photochromic part, it has been suggested that the synthetic hackmanites could be made into wearable UV detection tags that could help customers to follow their own UV exposure [IV]. Since the excitation spectrum for K-hackmanite follows the erythemal action spectrum of the human skin well, the color intensity in the UV tag could warn the carrier of too much exposure to harmful radiation. In addition to the use in personal health indication, similar tags with different activation energy could be prepared for other objects suffering from damage caused by UV, for example wine and beer, some food items and plastics.

Lastly, the addition of the up-conversion luminescence to the hackmanites resulted in one material with 4 different optical properties all excited with different wavelengths. Materials like this can be used in optical multiplexing, where one material gives different signals depending on what kind of radiation it is exposed to. In this way, for example, the wavelength (range) of an unknown

radiation source could be determined based on the mixture of optical signals obtained from the synthetic hackmanite after it has been exposed to the radiation (**Figure 41**).
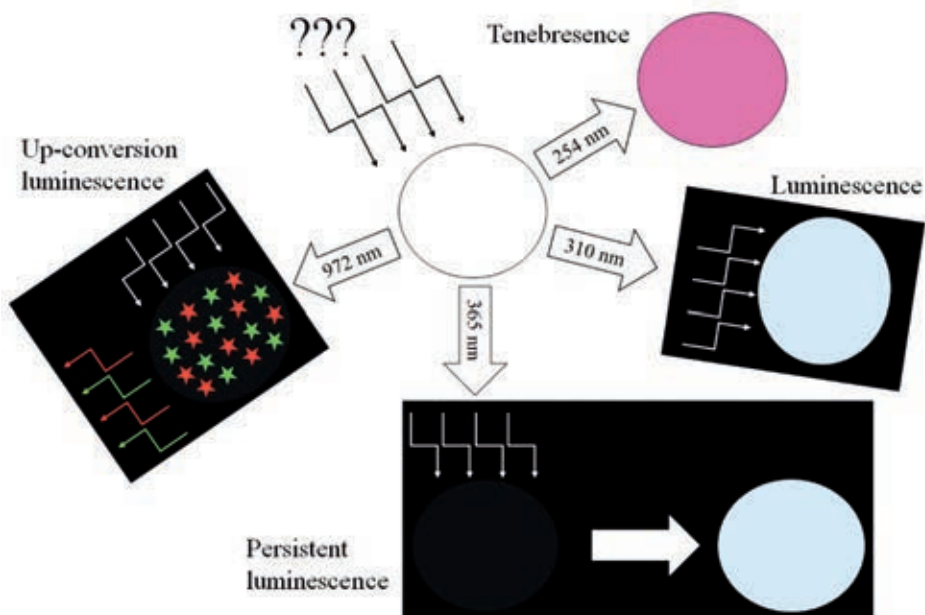
Figure 41 Shematic overwiev of the hackmanite material used in multiplexing determining the wavelenght of the unkonwn radiation.

The synthetic hackmanites have already many possible applications. Since the subject is still quite new and the research on synthetic hackmanites will still go on, other possible applications might come up even in the near future.

6. Summary

Synthetic Li-, Na-, K- and Rb-hackmanite materials were successfully prepared using solid state synthesis. Their chemical composition and crystalline structure were confirmed to be that of hackmanite using XRF and XPD measurements.

The synthetic hackmanite materials exhibited PL, PeL and photochromism. The color and the intensity of the luminescence as well as the photochromism could be tuned by adding dopants to the material. Ti doped Li-hackmanite showed the strongest luminescence. The color of the luminescence falls to white in CIE color coordinates and thus shows great potential in possible applications in lighting industries.

K- and Rb-hackmanites showed strong photochromism, and the activation energy for the phenomenon was tunable with different hackmanite compositions. The formation of F centers changes the body color of hackmanite from white to dark purple. The color change can be reversed with proper radiation or heating of the material. The material stays intact during the coloration and de-coloration cycles and they can be repeated numerous times.

Na-hackmanites doped with ytterbium and erbium were prepared resulting in hackmanite materials showing up-conversion luminescence. The results proved that the hackmanites can act as host materials for the up-conversion luminescence but more optimization would be needed to get the luminescence emission stronger.

In addition to the properties of the hackmanite materials, the mechanism was also studied. During the research a mechanism was proposed for both PeL and photochromism in synthetic hackmanites. The mechanism of PeL involves

titanium and oxygen vacancies forming in the material. The titanium can be doped or it can be found as an impurity in starting materials used in the hackmanite synthesis. For the photochromism mechanism, S_2^{2-} and V_{Cl} were found to be responsible.

The results obtained lead to many promising possibilities for commercial use for synthetic hackmanites. Lighting applications and UV monitoring are good examples for these kinds of applications and many more might appear in the future.

The current research gives a good basic understanding on the optical properties of the synthetic hackmanites. Next steps in the research should include the testing of different doping ions and the larger variation of the hackmanite structure to prepare materials with even stronger luminescence or different colors of photochromism. The solid state synthesis in use now works well in the laboratory conditions, although if moved to commercial use, the synthesis should be made shorter to save time and heating expenses. Because of this, different synthesis methods for hackmanites should be studied. Different methods could be for example combustion synthesis, microwave synthesis or liquid phase synthesis.

References

1. Zahoransky, T.; Friis, H.; Marks, M. A. W. Luminescence and tenebrescence of natural sodalites: a chemical and structural study. *Phys. Chem. Miner.* **2016**, *43*, 459–480.

2. Gaft, M.; Reisfeld, R.; Panczer, G. Sodalite $Na_8[Al_6Ai_6O_{24}]Cl_2$, Hackmanite $Na_8[Al_6Si_6O_{24}](Cl,S)$ and Tugtupite $Na_4AlBeSi_4O_{12}C$. In *Modern luminescence spectroscopy of minerals and baterials*; 2015; pp. 181–183.

3. Gaft, M.; Panczer, G.; Nagli, L.; Yeates, H. Laser-induced time-resolved luminescence of tugtupite, sodalite and hackmanite. *Phys. Chem. Miner.* **2009**, *36*, 127–141.

4. Warner, T. E. *Synthesis, properties and mineralogy of inportant inorganis materials*; John Wiley & Sons, 2012.

5. Allan, R. *A Manual of Mineralogy*; 1834.

6. Baur, W. H.; Fischer, R. X. A historical note on the sodalite framework: The contribution of Frans Maurits Jaeger. *Microporous Mesoporous Mater.* **2008**, *116*, 1–3.

7. Medved, D. B. The optical properties of natural and synthetic hackmanite. *J. Chem. Phys.* **1953**, *20*, 1309–1310.

8. Williams, E. F.; Hodgson, W. G.; Brinen, J. S. Synthetic Photochromic Sodalite. *J. Am. Ceram. Soc.* **1969**, *52*, 139–145.

9. Hodgson, W. G.; Brinen, J. S.; Williams, E. F. Electron Spin Resonance Investigation of Photochromic Sodalites. *J. Chem. Phys.* **1967**, *47*, 3719–3723.

10. Armstrong, J. A.; Weller, M. T. Structural observation of photochromism. *Chem. Commun.* **2006**, *10*, 1094–1096.

11. Williams, E. R.; Simmonds, A.; Armstrong, J. A.; Weller, M. T. Compositional and structural control of tenebrescence. *J. Mater. Chem.* **2010**, *20*, 10883–10887.

12. Warner, T. E.; Hutzen Andersen, J. The effects of sulfur intercalation on the optical properties of artificial 'hackmanite', $Na_8[Al_6Si_6O_{24}]Cl_{1.8}S_{0.1}$; 'sulfosodalite', $Na_8[Al_6Si_6O_{24}]S$; and natural tugtupite, $Na_8[Be_2Al_2Si_8O_{24}](Cl,S)_{2-\delta}$. *Phys. Chem. Miner.* **2012**, *39*, 163–168.

13. Kondo, D.; Beaton, D. Hackmanite/sodalite from Myanmar and Afghanistan. *Gems Gemol.* **2009**, *45*, 38–43.

14. Cano, N. F.; Blak, A. R.; Watanabe, S. Correlation between electron paramagnetic resonance and thermoluminescence in natural sodalite. *Phys. Chem. Miner.* **2010**, *37*, 57–64.

15. Peterson, R. C. The structure of hackmanite, a variety of sodalite, from Mont St-Hilaire, Quebec. *Can. Miner.* **1983**, *21*, 549–552.

16. Hassan, I.; Grundy, H. D.

Handbook of Mineralogy; 1983.

17. Hassan, I.; Grundy, H. D. The crystal structures of sodalite-group minerals. *Acta Crystallogr. Sect. B* **1984**, *B40*, 6–13.

18. Hassan, I.; Antao, S. M.; Parise, J. B. Sodalite: High-temperature structure obtained from synchrotron radiation and Rietveld refinements. *Am. Mineral.* **2004**, *89*, 359–364.

19. Goettlicher, J.; Kotelnikov, A.; Suk, N.; Kovalski, A.; Vitova, T.; Steininger, R. Sulfur K X-ray absorption near edge structure spectroscopy on the photochrome sodalite variety hackmanite. *ZEITSCHRIFT FUR Krist. Mater.* **2013**, *228*, 157–171.

20. Lee, O. I. A new property of matter: Reversible photosensitivity in hackmanite from Bancroft, Ontario. *Am. Mineral.* **1936**, *21*, 764–776.

21. Kirk, R. D. The Luminescence and Tenebrescence of Natural and Synthetic Sodalite. *Am. Mineral.* **1955**, *40*, 22–31.

22. Miser, H. D.; Glass, J. J. Fluorecent sodalite and hackmanite from Magnet Cove, Arkansas. **1941**, *26*, 437–445.

23. Gaft, M.; Reisfeld, R.; Panczer, G. *Modern luminescence spectroscopy of minerals and materials*; Springer, 2015.

24. Shionoya, S.; Yen, W. M.; Yamamoto, H. *Phosphor Handbook*; Weber, M. J., Ed.; 2nd ed.; CRC Press, 2006.

25. Hölsä, J. Persistent Luminescence Beats the Afterglow: 400 Years of Persistent Luminescence. *Electrochem. Soc. Interface* **2009**, *18*, 42–45.

26. Lastusaari, M.; Laamanen, T.; Malkamäki, M.; Eskola, K. O.; Kotlov, A.; Carlson, S.; Welter, E.; Brito, H. F.; Bettinelli, M.; Jungner, H.; Hölsä, J. The Bologna Stone: history's first persistent luminescent material. *Eur. J. Mineral.* **2012**, *24*, 885–890.

27. Blasse, G.; Grabmaier, B. C. *Luminescent Materials*; Springer-Verlag, 1994.

28. Blasse, G. *Handbook on the physics and chemistry of rare earths*; Elsevier, 1979.

29. Tamatani, M. Principal phosphor materials and their optical properties. In *Phosphor handbook*; CRC Press, 2006; pp. 167–188.

30. Jacobs, P. W. M. Alkali halide crystals containing impurity ions with the ns^2 ground-state electronic configuration. *J. Phys. Chem. Solids* **1991**, *52*, 36–67.

31. Tanimizu, S. Principal phosphor materials and their optical properties. In *Phosphor handbook*; CRC Press, 2006; pp. 155–165.

32. Seitz, F. Interpretation of the properties of alkali halide-thallium phosphors. *J. Chem. Phys.* **1938**.

33. Ranfagni, A.; Mugnai, D.; Bacci, M.; Viliani, G.; Fontana, M. P. The optical properties of thallium-like impurities in alkali-

halide crystals. *Adv. Phys.* **1983**, *32*, 823–905.

34. Rahman, A. Z. M. S. *Solid state luminescent materials: Applications*; Elsevier, 2016.

35. Williams, E. W.; Hall, R. *Luminescence and the light emitting diode*; Pamplin, B. R., Ed.; 1978.

36. Eliseeva, S. V.; Bünzli, J.-C. G. Lanthanide luminescence for functional materials and bio-sciences. *Chem. Soc. Rev.* **2010**, *39*, 189–227.

37. Franks, L. A.; Borella, H. M.; Lutz, S. S.; Turley, W. D.; Noel, B. W.; Beasley, A.; Allison, S. W.; Cates, M. R. Rare-earth phosphors for remote thermometry applications. *J. Electrochem. Soc.* **1987**, *134*, C491.

38. Xu, J.; Tanabe, S. Persistent luminescence instead of phosphorescence: History, mechanism, and perspective. *J. Lumin.* **2019**, *205*, 581–620.

39. Matsuzawa, T.; Aoki, Y.; Takeuchi, N.; Murayama, Y. A New Long Phosphorescent Phosphor with High Brightness, $SrAl_2O_4:Eu^{2+},Dy^{3+}$. *J. Electrochem. Soc.* **1996**, *143*, 2670–2673.

40. Yamamoto, H.; Matsuzawa, T. Mechanism of long phosphorescence of $SrAl_2O_4:Eu^{2+}$, Dy^{3+} and $CaAl_2O_4:Eu^{2+}$, Nd^{3+}. *J. Lumin.* **1997**, *72–74*, 287–289.

41. Lin, Y.; Tang, Z.; Zhang, Z.; Wang, X.; Zhang, J. Preparation of a new long afterglow blue-emitting $Sr_2MgSi_2O_7$-based photoluminescent phosphor. *Jurnlan Mater. Sci. Lett.* **2001**, *20*, 1505–1506.

42. Kang, C.; Liu, R.; Chang, J.-C.; Lee, B.-J. Synthesis and Luminescent Properties of a New Yellowish-Orange Afterglow Phosphor Y_2O_2S: Ti,Mg. *Chem. Mater.* **2003**, *15*, 3966–3968.

43. Clabua, F.; Rocquefelte, X.; Jobic, S.; Deniard, P.; Whangbo, M.-H.; Gracia, A.; LE Mercier, T. On the phosphorescence mechanism in $SrAl_2O_4:Eu^{2+}$ and its codoped derivatives. *Solid State Sci.* **2007**, *9*, 608–612.

44. Smet, P. F.; Botterman, J.; Van den Eeckhout, K.; Korthout, K.; Poelman, D. Persistent luminescence in nitride and oxynitride phosphors: A review. *Opt. Mater. (Amst).* **2014**, *36*, 1913–1919.

45. Singh, S. K. Red and near infrared persistent luminescence nano-probes for bioimaging and targering applications. *RSC Adv.* **2014**, *4*, 58674–58698.

46. Zhuang, Y.; Katayama, Y.; Ueda, J.; Tanabe, S. A brief review on red to near-infrared persistent luminescence in transition-metal-activated phosphors. *Opt. Mater. (Amst).* **2014**, *36*, 1907–1912.

47. Wang, X.; Zhang, Z.; Tang, Z.; Lin, Y. Characterization and properties of a red and orange Y_2O_2S-based long afterglow phosphor. *Mater. Chem. Phys.* **2003**, *80*, 1–5.

48. Shuanglong, Y.; Yunxia, Y.; Bin,

F.; Guorong, C. Effects of doping ions on afterglow properties of Y_2O_2S:Eu phosphors. *Opt. Mater. (Amst).* **2007**, *30*, 535–538.

49. Xu, J.; Ueda, J.; Kuroishi, K.; Tanabe, S. Fabrication of Ce^{3+}–Cr^{3+} co-doped yttrium aluminium gallium garnet transparent ceramic phosphors with super long persistent luminescence. *Scr. Mater.* **2015**, *102*, 47–50.

50. Li, Y.; Gecevicius, M.; Qiu, J. Long persistent phosphors — from fundamentals to application. *Chem. Soc. Rev.* **2016**, *45*, 2090–2136.

51. Poelman, D.; Smet, P. F. Photometry in the dark: time dependent visibility of low intensity light sources. *Opt. Express* **2010**, *18*, 26293–26299.

52. Lisensky, G. C.; Patel, M. N.; Reich, M. L. Experiments with glow-in-the-dark toys: Kinetics of doped ZnS phosphorescence. *J. Chem. Educ.* **1996**, *73*, 1048–1051.

53. Abdukayum, A.; Chen, J.-T.; Zhao, Q.; Yan, X.-P. Functional near infrared-emitting Cr^{3+}/Pr^{3+} co-doped zinc gallogermanate persistent luminescent nanoparticles with superlong afterglow for in vivo targeted bioimaging. *J. Am. Chem. Soc.* **2013**, *135*, 14125–14133.

54. Maldiney, T.; Ballet, B.; Bessodes, M.; Scherman, D.; Richard, C. Mesoporous persistent nanophosphors for in vivo optical bioimaging and drug-delivery. *Nanoscale* **2014**, *6*, 13970–13976.

55. Paterson, A. S.; Raja, B.; Garvey, G.; Kolhtkar, A.; Magström, A. E. V.; Kourentzi, K.; Lee, T. R.; Willson, R. C. Persistent luminescence strontium aluminate nanoparticles as reporters in lateral flow assays. *Anal. Chem.* **2014**, *86*, 9481–9488.

56. Van den Eeckhout, K.; Poelman, D.; Smet, P. F. Persistent Luminescence in Non-Eu^{2+}-Doped Compounds: A Review. *Materials (Basel).* **2013**, *6*, 2789–2818.

57. Guangbo, C.; Chunbo, L.; Qingwei, W.; Zhanlin, X. White-light-emission Afterglow Phosphor $CaZnGe_2O_6$:Dy^{3+}. *Chem. Lett.* **2008**, *37*, 136–137.

58. Rodrigues, L. C. V.; Hölsä, J.; Lastusaari, M.; Felinto, M. C. F. C.; Brito, H. F. Defect to R^{3+} energy transfer: colour tuning of persistent luminescence in $CdSiO_3$. *J. Mater. Chem. C* **2014**, *2*, 1612–1618.

59. Xu, X.; Wang, Y.; Zeng, W.; Gong, Y.; Liu, B. Luminescent properties of the multicolor afterglow phosphors $Ca_3SnSi_2O_9$:Re^{3+} (Re = Pr, Tb, Sm). *J. Am. Ceram. Soc.* **2011**, *94*, 3632–3635.

60. Gong, Y.; Wang, Y.; Li, Y.; Xu, X. Ce^{3+}, Dy^{3+} co-doped white-light long-lasting phosphor: $Sr_2Al_2SiO_7$ through energy transfer. *J. Electrochem. Soc.* **2010**, *157*, J208–J211.

61. Feng, L.; Wang, Z.; Cao, C.; Zhang, T.; Zhang, J.; CI, Z.; Zhao, Z.; Wang, Y. Warm-white

persistent luminescence of $Lu_3Al_2Ga_3O_{12}:Pr^{3+}$ phosphor. *J. rare earths* **2017**, *35*, 47–52.

62. Zhang, Q.; Rong, M.; Tan, H.; Wang, Z.; Wang, Q.; Zhou, Q.; Chen, G. Luminescent properties of the white long afterglow phosphors: $Sr_3Al_2O_5Cl_2:Eu^{2+}$, Dy^{3+}. *J. Mater. Sci. Mater. Electron.* **2016**, *27*, 13093–13098.

63. Auzel, F. Upconversion and Anti-Stokes Processes with f and d Ions in Solids. *Chem. Rev.* **2004**, *104*, 139–173.

64. Carnall, W. T.; Goodman, G. L.; Rajnak, K.; Rana, R. S. A systematic analysis of the spectra of the lanthanides doped into single crystal LaF3. *J. Chem. Phys.* **1989**, *90*, 3443–3457.

65. Wang, H.-Q.; Batentschuk, M.; Osvet, A.; Pinna, L.; Brabec, C. J. Rate-earth ion doped up-conversion materials for photovoltaic applications. *Adv. Mater.* **2011**, *23*, 2675–2680.

66. Arppe, R.; Näreoja, T.; Nylund, S.; Mattsson, L.; Koho, S.; Rosenholm, J. M.; Soukka, T.; Schäferling, M. Photon upconversion sensitized nanoprobes for sensing and imaging of pH. *Nanoscale* **2014**, *6*, 6837–6843.

67. Yi, G.; Lu, H.; Zhao, S.; Ge, Y.; Yang, W.; Chen, D.; Guo, L.-H. Synthesis, characterization, and biological application of size-controlled nanocrystalline $NaYF_4:Yb,Er$ infrared-to-visible up-conversion phosphors. *Nano Lett.* **2004**, *4*, 2191–2196.

68. Irie, M. Photochromism:

Memories and Switches - Introduction. *Chem. Rev.* **2000**, *100*, 1683–1684.

69. Bouas-Laurent, H.; Dürr, H. Organic photochromism (IUPAC tecnical report). *Pure Appl. Chem.* **2001**, *73*, 639–665.

70. Medved, D. B. Hackmanite and its tenebrescent properties. *Am. Mineral.* **1954**, *39*, 615–629.

71. Mitchell, J. W. XXIII. The properties of silver halides containing traces of silver sulphide. *London, Edinburgh, Dublin Philos. Mag. J. Sci.* **1949**, *40*, 249–268.

72. Smakula, A. Color Centers in Calcium Fluoride and Barium Fluoride Crystals. *Phisical Rev.* **1950**, *77*, 408–409.

73. Pough, F. H.; Rogers, T. H. Experiments in X-ray irradiation of gem stones. *Am. Mineral.* **1974**, *32*, 31–43.

74. Weyl, W. A.; Förland, T. Photochemistry of rutile. *Ind. Eng. Chem.* **1950**, *42*, 257–263.

75. Kawata, S.; Kawata, Y. Three-dimensional optical data storage using photochromic materials. *Chem. Rev.* **2000**, *100*, 1777–1788.

76. Raymo, F. M.; Tomasulo, M. Fluorescence modulation with photochromic switches. *J. Phys. Chem. A* **2005**, *109*, 7343–7352.

77. Dorofeeva, N. P.; Zak, P. P.; Tsekhomskii, V. A. Photochromic-glasses for eyeglass optics. *J. Opt. Technol.* **1994**, *61*, 891–893.

78. Cheng, T.; Lin, T.; Fang, J.; Brady, R. Photochromic wool fabrics from a hybrid silica coating. *Text. Res. J.* **2007**, *77*, 923–928.

79. Lastusaari, M.; Norrbo, I. Synthetic material for detecting ultraviolet radiation and/or x-radiation, WO 2017/194834 A1.

80. Kirk, R. D. Role of sulfur in the luminescence and coloration of some aluminosilicates. *J. Electrochem. Soc.* **1954**, *101*, 461–465.

81. Borgström, L. H. Hackmanit ett nytt mineral i sodalitgruppen. *Geol. För. Stock.* **1901**, *23*, 563–569.

82. Vredenburg, E. Elaeolite and soda syenites in kishengarh state, Rajputana, India. *Rec. Geol. Sorvey India* **1904**, *31*, 43–44.

83. Taylor, M. J.; Marshall, D. J.; Forrester, P. A.; McLaughlan, S. D. Colour centers in sodalites and their use in storage displays. *Radio Electron. Eng.* **1970**, *40*, 17–25.

84. Etsy.com Natural Hackmanite UV Colorchange Ring Sterling 925 Available online: https://www.etsy.com/listing/634004557/natural-hackmanite-uv-colorchange-ring?ga_order=most_relevant&ga_search_type=all&ga_view_type=gallery&ga_search_query=hackmanite+jewelry&ref=sr_gallery-1-9 (accessed on Feb 1, 2019).

85. Mikuła, A.; Król, M.; Koleżyński, A. Experimental and theoretical spectroscopic studies of Ag- , Cd- and Pb- sodalite. *J. Mol. Struct.*
2016, *1126*, 110–116.

86. Chong, S.; Peterson, J.; Nam, J.; Riley, B.; McCloy, J. Synthesis and characterization of iodosodalite. *J. Am. Chem. Soc.* **2017**, *100*, 2273–2284.

87. Buhl, J.-C.; Gesing, T. M.; Gurris, C. Synthesis and crystal structure of rhodanide-enclathrated sodalite $Na_8[AlSiO_4]_6(SCN)_2$. *Microporous Mesoporous Mater.* **2001**, *50*, 25–32.

88. Johnson, G. M.; Mead, P. J.; Weller, M. T. Synthesis of a range of anion-containing gallium and germanium sodalites. *Microporous Mesoporous Mater.* **2000**, *38*, 445–460.

89. Carvalho, J. M.; Norrbo, I.; Ando, R. A.; Brito, H. F.; Fantini, M. C. A.; Lastusaari, M. Fast , low-cost preparation of hackmanite minerals with reversible photochromic behavior using a microwave-assisted structure-conversion method. *Chem. Commun.* **2018**, *54*, 7326–7329.

90. International Centre for Diffraction Data, PDF-4+ 2013, 00-002-0351.

91. International Centre for Diffraction Data, PDF-4+ 2013, 01-080-3939.

92. Rietveld, H. M. A Profile Refinement Method for Nuclear and Magnetic Structure. *J. Appl. Crystallogr.* **1969**, *2*, 65–71.

93. Rodriguez-Carvajal, J. FullProf.2k Version 5.30 - Mar2012, Laboratoire Leon Brillouin (CEA.CNRS), Gif-sur-

Yvette, France 2012.

94. Rodriguez-Carvajal, J. FullProf.2k Version 5.70 - Nov2015, Laboratoire Leon Brillouin (CEA-CNRS), Gif-sur-Yvette, France 2015.

95. Rodríguez-Carvajal, J. Recent advances in magnetic structure determination by neutron powder diffraction. *Phys. B Condens. Matter* **1993**, *192*, 55–69.

96. Schneider, C. A.; Rasband, W. S.; Eliceiri, K. W. NIH Image to ImageJ : 25 years of image analysis. *Nat. Methods* **2012**, *9*, 671–675.

97. CASAXPS: Processing Software for XPS, AES, SIMS, and more, version 2.3.16 Casa Software Ltd. 2016.

98. *Phosphorescent Pigments and Products - Part 1: Measurement and Marking at the Producer, DIN 67510-1:2009-11*; Berlin, Germany, 2009.

99. Chen, R.; McKeever, S. W. S. *Theory of Thermoluminescence and Related Phenomena*; World Scientific: Singapore, 1997.

100. Van Den Eeckhout, K.; Bos, A. J. J.; Poelman, D.; Smet, P. F. Revealing trap depth distributions in persistent phosphors. *Phys. Rev. B - Condens. Matter Mater. Phys.* **2013**, *87*, 045126-1–11.

101. Becke, A. D. Perspective: Fifty years of density-functional theory in chemical physics. *J. Chem. Phys.* **2014**, *140*, 18A301.

102. Fischer, C. F. General Hartree-Fock program. *Comput. Phys. Commun.* **1987**, *43*, 355–365.

103. Kohn, W.; Sham, L. J. Self-consistent equations including exchange and correlation effects. *Phys. Reviev* **1965**, *140*, A1133–A1138.

104. Shannon, R. D. Revised Effective Ionic Radii and Systematic Studies of Interatomic Distances in Halides and Chalcogenides. *Acta Crystallogr. Sect. A* **1976**, *32*, 751–767.

105. Trill, H.; Eckert, H.; Srdanov, V. I. NMR study of interacting F centers in $Na_8[Al_6Si_6O_{24}]Cl_2$ sodalite. *Phys. Rev. B* **2005**, *71*, 014412.

106. Buhl, J.-C.; Schuster, K.; Robben, L. Nanocrystalline sodalite grown from superalkaline NaCl bearing gels at low temperature (333 K) and the influence of TEA on crystallization process. *Microporous Mesoporous Mater.* **2011**, *142*, 666–671.

107. Van Doorn, C. Z.; Schipper, D. J. Luminescence of O_2^-, Mn^{2+} and Fe^{3+} in sodalite. *Phys. Lett.* **1971**, *34*, 139–140.

108. Fortner, B.; Meyer, T. E. *Defining Colors - The CIE Color Diagram in Number by Colors*; Springer, New York, NY, 1997.

109. Kasprowicz, D.; Gluchowski, P.; Brik, M. G.; Makowski, M. M.; Chrunik, M.; Majchrowski, A. Visible and near-infrared up-conversion luminescence of $KGd(WO_4)_2$ micro-crystals doped with Er^{3+}, Tm^{3+}, Ho^{3+} and Yb^{3+} ions. *J. Alloys Compd.* **2016**, *684*, 271–281.

Annales Universitatis Turkuensis

UNIVERSITY OF TURKU